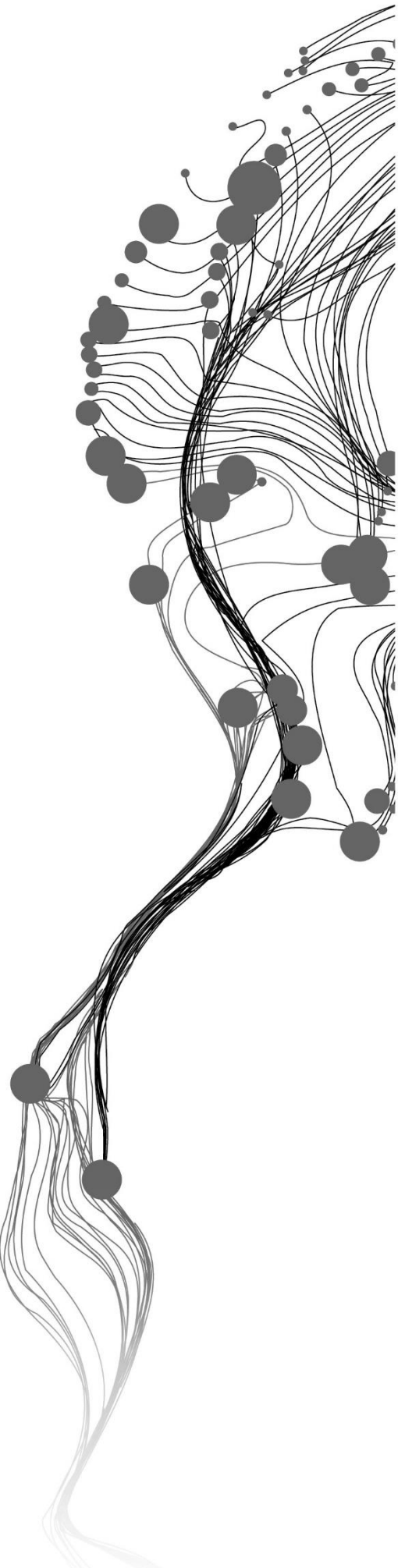


SPATIAL PREDICTIVE MODELING FOR OUTLINING AREAS PRONE TO TORRENTIAL FLOWS IN THE COLOMBIAN ANDES

MATEO MORENO ZAPATA
AUGUST, 2021

SUPERVISORS:
Dr. L. Lombardo
Prof. dr. C.J. van Westen



SPATIAL PREDICTIVE MODELING FOR OUTLINING AREAS PRONE TO TORRENTIAL FLOWS IN THE COLOMBIAN ANDES

MATEO MORENO ZAPATA
Enschede, The Netherlands, August 2021

Thesis submitted to the Faculty of Geo-Information Science and Earth Observation of the University of Twente in partial fulfilment of the requirements for the degree of Master of Science in Geo-information Science and Earth Observation.

Specialization: Natural Hazards and Disaster Risk Reduction

SUPERVISORS:

Dr. L. Lombardo

Prof. dr. C.J. van Westen

THESIS ASSESSMENT BOARD:

Prof. dr. N. Kerle (Chair)

Dr. S. Steger (External Examiner, Eurac Research)

DISCLAIMER

This document describes work undertaken as part of a programme of study at the Faculty of Geo-Information Science and Earth Observation of the University of Twente. All views and opinions expressed therein remain the sole responsibility of the author, and do not necessarily represent those of the Faculty.

ABSTRACT

Historical records show the highly destructive power that torrential flows have had in the Colombian Andes. In the current climate change scenario, frequencies and intensities of extreme events are expected to increase in the upcoming years, likely leading to an increase in torrential flow events. Despite each municipality in Colombia requires susceptibility assessment of torrential flow as a basis for the land use planning, very few studies have been done at a national scale in Colombia. Besides, a recent methodological guide for assessing torrential flow describes methods that require detailed information which cannot be applied to the entire Colombian territory. Therefore, prioritizing the watersheds where detailed torrential flow hazard analysis should be applied is a crucial first step for spatial planning purposes. This research applied Generalized Additive Models in a Bayesian framework to model torrential flow susceptibility at a national scale in Colombia. Different watershed levels were considered to find a suitable representation of these phenomena. Two inventories, DesInventar and SIMMA were used for the susceptibility model. The predisposing and triggering factors were grouped into morphometric indices, lithology, land cover-land use, and rainfall. Validation and performance estimations were assessed with the Area Under the Receiver Operating Characteristics (AUROC) using a k-fold cross-validation. The results were classified into five classes according to the success rate curves. Afterward, the selected levels of watersheds were combined with different Elements at Risk (urban centers and small settlements) to prioritize areas prone to torrential flows. In terms of the predictor variables, slope and maximum daily rainfall showed the highest contributions to the susceptibility models. Also, the obtained performances (median AUROC from 0.82 to 0.87) suggest a relatively high predictive power for all the watershed levels. The integration with the EaR showed a total of 871 watersheds out of 32,293 (with an area of 21,600 km²) for the most detailed level (Level 1-1,000) were in the highest priority class. At the second level of detail (Level 2 -5,000) the results showed that in 429 watersheds out of 6,906 with an estimated area of 51,900 km² where more detailed studies should be carried out.

Keywords: Torrential flows, Data-driven models, Susceptibility, Urban planning

ACKNOWLEDGEMENTS

This work could not have been possible without all people who were part of this fantastic two-year journey. My deep thanks to everyone. First, I would like to express my eternal appreciation to my beloved family, my mom, brother, and dad, who continuously supported and encouraged me no matter how challenging the circumstances were.

I want to give special thanks to my supervisors at ITC, Luigi Lombardo, and Cees van Westen for all the guidance, advice, time, support, inspiration, and constructive feedback during the MSc thesis period and courses.

My thankfulness to Serkan Girgin for the help with the Geospatial Computing Platform, which was a fundamental step along with the entire research work.

Thank you, Luisa; even from the distance, your time and support during this thesis were very much valued and appreciated.

I could not be more grateful to King for your endless help, care, love, and always being there with me when I needed it the most. I thank all my friends who always treated me like family: Ishmam, Om, Diana, Boo, Ash-ok, Lucia, Maria, Nestor, Ana, Anny, and many others (you guys know whom you are (;)). Thank you for being there, for the fun times we shared together. I hope you all walk to the future you want, and I hope to see you soon again.

TABLE OF CONTENTS

1.	INTRODUCTION.....	10
1.1.	Background.....	10
1.2.	Problem statement	11
1.3.	Research objectives	12
2.	CONCEPTUAL FRAMEWORK.....	14
2.1.	Debris flow concept.....	14
2.2.	Susceptibility and hazard models.....	15
2.3.	Generalized Additive Models (GAMs).....	16
3.	STUDY AREA	18
3.1.	Location	18
3.2.	Geomorphological and geological settings	19
3.3.	Administrative context	19
4.	DATA.....	22
4.1.	Inventory.....	22
4.2.	Digital Elevation Model (DEM).....	25
4.3.	Thematic predisposing factors	26
4.4.	Triggering factors	30
4.5.	Cartographic base	31
4.6.	Watersheds.....	31
5.	METHODS.....	33
5.1.	Watershed generation	34
5.2.	Role of the predisposing and triggering factors in the occurrence of torrential flow events	34
5.3.	Suitable basic mapping unit to represent torrential flow susceptibility	37
5.4.	Prioritization of areas prone to torrential flows.....	37
6.	RESULTS	39
6.1.	Watershed generation	39
6.2.	Role of the predisposing and triggering factors in the occurrence of torrential flow events	41
6.3.	Suitable basic mapping unit to represent torrential flow susceptibility	44
6.4.	Prioritization of areas prone to torrential flows.....	47
7.	DISCUSSION.....	53
7.1.	Covariate effects	53
7.2.	Suitable mapping unit to model to represent torrential flow susceptibility	54
8.	CONCLUSIONS	56
9.	ETHICAL CONSIDERATIONS.....	57
10.	APPENDIX	63
10.1.	Land cover parametrization.....	63
10.2.	Potential land use.....	64
10.3.	Daily rainfall data preparation	65
10.4.	Annual rainfall data preparation	66
10.5.	Watershed generation	68
10.6.	Terrain derivatives calculation and aggregation procedure.....	69
10.7.	Multi-collinearity test	70
10.8.	Multi-collinearity test for Geology	70
10.9.	Multi-collinearity test for rainfall	70
10.10.	Multi-collinearity test for land cover and land use	71
10.11.	Posterior 95% CI vs. posterior mean susceptibilities for all the watershed levels and models	72

LIST OF FIGURES

Figure 1. Location and physiographical overview of Colombia..	18
Figure 2. On the left side, the geological map of Colombia at a scale 1:1,000,000. The colors follow the International Chronostratigraphic Chart, and the detailed map and legend are available in the interactive application provided by SGC. On the right side, the geomorphological provinces describe by Carvajal-Perico (2012). The boundary in red corresponds to the region of interest.....	21
Figure 3. Location of the study area showing the three considered inventories and the region of interest (red boundary) based on the proposed standardization for the geomorphological cartography in Colombia.	23
Figure 4. Visual comparison between SIMMA (magenta triangles) and DesInventar (white dots).....	25
Figure 5. Land cover map (left side) and potential land use map (right side).....	29
Figure 6. ImageCollection reduction functions (ee.Reducer) in GEE. Modified from https://developers.google.com/earth-engine	30
Figure 7. Total annual rainfall for a time window from 1980 to 2020. The bar in green represents the year with the maximum total annual precipitation.	31
Figure 8. Temporal aggregation of the rainfall. From left to right, the total rainfall for the year with the maximum annual rainfall (2011), maximum daily rainfall, and mean daily rainfall.	32
Figure 9. General overview of the methods.....	33
Figure 10. Influence of watershed geometry in the hydrograph. Modified of echo2.epfl.ch	34
Figure 11. Scheme of the watershed generation process	39
Figure 12. Overview of the different levels of delineated watersheds. From left to right and from top to bottom, watershed level 50,000, 25,000, 10,000, 5,000 and 1,000.....	40
Figure 13. Multi-collinearity test for morphometric indices. Abbreviations according to Table 8. >0.75 or >-0.75 were taken as thresholds to indicate whether the pair of covariates show strong relations or not..	41
Figure 14. Linear effects (significant) for Mod1 and Mod2. The y-axis reports the covariates with the respective regression coefficients in the x-axis. Diamonds depict the mean of the posterior distribution for each RC. Triangles show the 95 credible intervals of the RC posterior distribution. In red, the negative mean RCs, in blue, the positive ones. The grey boxes divide the covariates into the previously established groups (morphometric indices, lithology, land cover-land use, and rainfall).....	43
Figure 15. Non-linear effects in the susceptibility models. The blue line summarizes the mean of the posterior distribution for the RC, and the black lines are the 95% credible interval.	44
Figure 16. Illustration of the ROC curves (Mod1). Every solid line represents the ROC curve associated with each one of the ten folds. The dashed line shows a theoretical random model (with AUROC = 0.5).	45
Figure 17. Posterior 95% CI vs. posterior mean susceptibility for the watersheds at level 1,000. Blue corresponds to Mod1 and red to Mod2.....	46
Figure 18. Posterior 95% CI vs. posterior mean susceptibility for Mod3.....	46
Figure 19. Success rate for Mod3. The color palette represents the previously established classes in Table 9.	47
Figure 20. Results for the watersheds in Level 1-50,000. The map on the left side shows the torrential flow susceptibility classes for Mod3, whereas the map on the right indicates the corresponding 95% credible interval.....	48
Figure 21. Results for the watersheds in Level 2-25,000 (top) and Level 3-10,000 (bottom). The map on the left side shows the torrential flow susceptibility classes for Mod3, whereas the map on the right indicates the corresponding 95% credible interval.....	49

Figure 22. Results for the watersheds in Level 4-5,000 (top) and Level 5-1,000 (bottom). The map on the left side shows the torrential flow susceptibility classes for Mod3, whereas the map on the right indicates the corresponding 95% credible interval. 50

Figure 23. Comparative overview of the different watershed levels. Note that since the levels 50,000 and 25,000 were equal (particularly for this area), they refer to the same panel. 51

Figure 24. Prioritized watersheds for levels 1,000 (left side) and 5,000 (right side) for Mod3. 52

Figure 25. Watershed subdivisions. Modified from <https://www.nps.gov/subjects/geology/fluvial-landforms.htm>..... 55

LIST OF TABLES

Table 1. Examples of the different sets of techniques to evaluate landslide susceptibility and hazard.	15
Table 2. Summary of the different datasets used during this research. The symbol (-) indicates that the information was not available and therefore could not be retrieved.	22
Table 3. Uncertainty level estimation for the spatial location of the DesInventar inventory.	24
Table 4. Summary of the used inventories according to the type of torrential flow. The numbers shown correspond to the filtered data (by uncertainty) used for the susceptibility model.	25
Table 5. Example of the disaggregation procedure for the lithological map. On the left side, the original lithological units, on the top, eight of the twenty-five base classes. 1/0 is used to represent the presence/absence of the base class in the respective lithological unit.	26
Table 6. Example of the reclassification for the land cover map. In the original level, the number of digits corresponds to the detail of the level. Therefore, three digits represent level 3.	27
Table 7. Example of the reclassification of the land use map.	30
Table 8. Summary of morphometrical indices included in the analysis. WL* stands for the watershed length. P* refers to the watershed perimeter. SN* is the number of streams. SL* stands for stream length. M stands for the average, and σ stands for the standard deviation.	36
Table 9. Susceptibility ranges based on the analysis of the success rates.	37
Table 10. Compilation of the generated watersheds. The number in the first columns corresponds to the minimum size of the exterior watershed basin.	40
Table 11. Report of the performance results. Median AUROC values are shown for Mod1 and Mod2 for all levels of watersheds.	45
Table 12. Report of the performance results. Median AUROC values are shown for Mod3 for all levels of watersheds.	46
Table 13. Percentage of susceptibility classes for each watershed level (Mod3).	47

LIST OF ABBREVIATIONS

SGC – Servicio Geológico Colombiano (Colombian Geological Survey)

GLM – Generalized Linear Model

GAM – Generalized Additive Model

ROC – Receiver Operating Characteristic

AUROC – Area Under the Receiver Operating Characteristics

SIMMA – Sistema de Información de Movimientos en Masa (Mass Movement Information System)

EaR – Element at Risk

GIS – Geographic Information System

GMS – Geomorphostructure

POT – Plan de Ordenamiento Territorial (Land Use Plan)

GEE – Google Earth Engine

IDEAM – Instituto de Hidrología, Meteorología y Estudios Ambientales (Institute of Hydrology, Meteorology and Environmental Studies)

PUJ – Pontificia Universidad Javeriana (Pontifical Xaverian University)

CV – Cross-validation

DEM – Digital Elevation Model

SR – Success rate

CHIRPS – Climate Hazards center InfraRed Precipitation with Station data

1. INTRODUCTION

This chapters covers the general research idea with the corresponding background (1), problem statement (2), and (3) research objectives with the respective research questions.

1.1. Background

Yearly, all around the world, a large number of human casualties result from the occurrence of different natural hazards like earthquakes, landslides, wildfires, and floods. According to The International Disasters Database of the Centre for Research on the Epidemiology of Disaster (EM-DAT), 330 disasters were triggered by hydro-meteorological extremes in 2019, resulting in 11.266 fatalities and affecting 73.1 million people, with total damages of 96.3 billion USD. Froude and Petley (2018), also based on data from EM-DAT for the years 1990 to 2015, showed that in comparison to other natural disasters, landslides are equivalent to 4.9% of all-natural disaster events, accounting for 1.3% of all the natural disaster fatalities in the mentioned time window. Within the landslide group, debris flows are often considered one of the most devastating types of events in terms of damage and losses. Dowling and Santi (2013) built a global-scale database for 1950-2011, where they compiled 213 events and found 77.779 associated fatalities.

Different flow-like landslide classification schemes have been proposed before. For example, Hungr and Jakob (2005) defined the term *debris flow* as a flow-like movement that consists of a mixture of water and sediments in different proportions descending downslope at extremely rapid velocities (several tens of km/h) with a long runout (from tens of m up to several km). The type of sediment, which can vary from cohesive material to granular, and even coarse boulders, along with the proportion of water, gives the debris flow their distinct characteristics. Furthermore, the relation of sediment/water, type of material, and triggering may give a place to some other variants of this phenomenon, better known as mud flows and debris floods (Hungr, Leroueil, & Picarelli, 2014). For this study, the debris flows and the variant processes which resulted in changes of the water/sediment ratio and type of sediments are referred to as *torrential flows* following the term in Spanish *avenidas torrenciales*. It is essential to highlight the importance of flow velocity in terms of destructive power. The faster the flow, the more sediments it can transport, and the larger the objects it can move. This destructive power has been evidenced across the world, resulting in many casualties and substantial economic losses.

At a continental scale, the impact of torrential flows is remarkable. Some examples can be found in Peru with the Chosica debris flow (see, e.g., Villacorta, Evans, Nakatani and Villanueva, (2020)) or the Glacial Lake Outburst Flood (GLOF) in the Cordillera Blanca, which in 1941 claimed 5,000 lives (Carey, 2008). There are also records of large events near Lake Ranco in Chile in 1991, 1993, and 2004 (see, e.g., Sepúlveda, Rebolledo and Vargas (2006)), in Venezuela, the Vargas tragedy, which caused an estimated death toll of 19,000 people and economic losses by 1.79 billion U.S. (Larsen, Wiczorek, Eaton, Morgan, & Torres-Sierra, 2001). At a country scale, Colombia has been impacted by numerous torrential flow events. Based on the Disaster Inventory System (DesInventar), Colombia has a record of 1,356 small to mid-size torrential flow events in the time window of 1921 to 2018, causing 3,318 deaths (Arango, Aristizábal, & Gómez, 2020). Besides, examples of significant events took place in Putumayo in 2017 with 332 casualties, Salgar in 2015 with 93 casualties, El Playón (1979) with 200 casualties, and the Armero tragedy in 1985 with a record of more than 22,000 deaths (Aristizábal, Arango, & López, 2020; Voight, 1990). These examples serve as proof and illustrate the need to incorporate measures to avoid losses.

In general, an important portion of the damage caused by torrential flows can be avoided if the exposure is reduced. Nevertheless, to achieve a decrease in the exposure, at least spatial predictive models that show where the events are expected to occur should be developed (Guzzetti, Reichenbach, Cardinali, Galli, & Ardizzone, 2005). The inclusion of susceptibility models can be considered a fundamental step for the appropriate risk reduction planning, including the set-up of risk mitigation measures (Hervás & Bobrowsky, 2009; Nadim, Kjekstad, Peduzzi, Herold, & Jaedicke, 2006). Creating a susceptibility model requires understanding the phenomenon's behavior and in-depth knowledge of its causative factors. To illustrate this, the spatial probability of torrential flows can be described through parameters such as lithology, land cover, and different morphometrical features. Also, rainfall, earthquakes, volcanic activity, snow-melting among others play essential roles since they may directly act as triggering factors; however, their spatial/temporal distribution is often more difficult to assess (Aristizábal & Sánchez, 2020; Zhang, Zhang, & Glade, 2014).

This research aims to estimate torrential flow susceptibility by implementing spatial predictive models at a national scale in Colombia. The Integrated Nested Laplace Approximation approach (INLA) is proposed to address the aforementioned goal. *INLA*, introduced by Rue, Martino and Chopin (2009), is a novel approach that makes Bayesian inference faster. "INLA relies on a combination of analytical approximations and efficient numerical integration schemes to achieve highly accurate and deterministic approximation to posterior quantities of interest" (Martino & Riebler, 2019, p. 1). This robust approach, which can be employed in R through the package *R-INLA*, is used to model the torrential flow susceptibility by implementing Generalized Additive Models (GAM). Previous studies which used this model design have shown optimal results (e.g. (Lombardo, Opitz, & Huser, 2018)).

1.2. Problem statement

In the current climate change context, frequencies and intensities of extreme events are expected to increase in the upcoming years, boosting the number of natural hazards (Güneralp, Güneralp, & Liu, 2015). Thus, the accurate estimation of the hazard and risk components could significantly reduce uncertainties in the whole risk assessment cycle and, consequently, reduce losses in the future. Furthermore, the accelerated growth of the population has led to an increase in the number of people affected by natural hazards as well as economic losses. Many regions of the world have then become subject to multiple hazards. Hence, decision-makers face the challenge of designing and implementing adequate risk assessments due to single hazards and multi-hazards (Komendantova et al., 2014). In September 2015, the General Assembly adopted the 2030 Agenda that includes 17 Sustainable Development Goals (SDGs) in which disaster reduction plays an important role in 10 of these goals, making the hazard assessments a relevant topic to be explored.

There are approaches which have provided initial schemes for risk management and urban planning at a national level in Colombia. In 2012, the Geological Survey of Colombia (SGC for its abbreviation in Spanish) proposed and developed the project under the translated name of "*Landslide relative hazard map at a national level 1:100.000 scale*" (SGC, 2012). The implemented methodology in that project was based on a multi-criteria/heuristic method known as the Analytic Hierarchy Process (AHP). In this method, decisions are taken using weights through pair-wise relative comparisons without inconsistencies in the decision process (Kayastha, Dhital, & De Smedt, 2013). To generate the landslide susceptibility map, this project considered predisposing factors based on morphometric characteristics, lithology, soil types, and land cover (SGC, 2012). Triggers, mainly rainfall and seismic load, were incorporated through arithmetic operations resulting in a relative hazard map. However, accuracy and uncertainty for the hazard model could not be quantitatively evaluated since there was no landslide inventory when the project was carried

out. Certainly, heuristic approaches are practical since they can be easily implemented but complex because they require extensive expert knowledge. Such approaches can be used to model landslides caused by different mechanisms together as opposed to other frameworks (Ruff & Czurda, 2008). They can also be used when no data are available to estimate susceptibility using data-driven or physically-based models. Multiple and more sophisticated approaches have been used to prioritize areas prone to torrential flows at a regional and municipal scale.

Different authors have used machine learning techniques to perform variable selection of morphometric parameters at a regional scale, aiming to distinguish torrential and non-torrential watersheds (Arango et al., 2020). Some others have focused on developing indices based on watershed parameters and land cover features to distinguish watersheds prone to different types of torrential flows and their spatial probability (Rogelis & Werner, 2014). There are complex approaches based on the integration of discriminant analysis to assess the debris flow spatial probability, logistic regression to account for the temporal probability, and physically-based models to include the flow magnitude (e.g., (Aristizábal, Arango, Gómez, et al., 2020)). Nevertheless, there has not been any spatial assessment of susceptibility or hazard of torrential flows at a national scale. Moreover, recently, a methodological guide to assessing torrential flow hazard at scales of 1:25,000, 1:2,000, and its incorporation with the land use planning is being produced (SGC & PUJ, 2020). The guide outlines a detailed procedure using physically-based models that involves a large amount of high-resolution data, which is challenging to adapt for many locations in Colombia. Therefore, having a pre-screening assessment that can indicate whether specific watersheds or mapping units are prone to debris flow or not is indeed helpful.

To summarize, the problem statement addresses that Colombia currently does not count with a national level assessment of torrential flow susceptibility. Several attempts have been made in small to medium size study areas. At a national level, the best approximation is a relative landslide hazard map that does not consider the distribution of past events nor the differentiation between torrential flows and other mass movements. Also, a new guide for torrential flow hazards at medium and detailed scales has been recently issued. Nevertheless, there is still the need to zoom into those areas so that the methods stated in the guide can be implemented. Having such susceptibility assessment at a national scale would indeed help in prioritizing specific areas and focusing efforts on more detailed analyses in them

1.3. Research objectives

This research exploits novel spatial predictive modeling approaches to generate a prioritization for watersheds prone to torrential flows at a national scale in Colombia. This general objective is subdivided into three sub-objectives which were addressed through their associated research questions.

1.3.1. To understand the role that the predisposing and triggering factors play in the occurrence of torrential flow events

- Which predisposing factors should be included in the torrential flow susceptibility model?
- What is the contribution and meaning of the predisposing factors in the torrential flow model?

1.3.2. To find a suitable basic mapping unit when estimating torrential flow susceptibility at a national scale in Colombia.

- How can the different mapping units influence the model outcomes, i.e., performance/uncertainty of the torrential flow susceptibility model?
- Which level of mapping unit can be best used to represent torrential flow susceptibility, given the available historical data, predisposing, and triggering factors?

- 1.3.3. **To prioritize areas prone to torrential flow by integrating the outcomes of the susceptibility model and land-use features.**
- How can the outcomes in the susceptibility map be interpreted and classified to achieve an optimal classification?
 - How can the results of susceptibility model be used in the analysis of torrential flow hazard for spatial planning purposes?

2. CONCEPTUAL FRAMEWORK

This chapter describes the literature review divided into (1) debris flow concept, (2) susceptibility and hazard models, and (3) Generalized Additive Models.

2.1. Debris flow concept

Classification schemes for debris flow have been discussed and have evolved in the literature over time. Initially, Cruden and Varnes (1996) provided a landslide classification scheme based on material and movement type. According to their proposed system, debris flow could be every flow-like movement where the material was predominantly coarse granular soils (debris), which opened an extensive discussion since this concept would include short phases of other landslide types. The term was adjusted by adding the constraints that debris flow must have extremely rapid velocities, flow through a confined steep channel, and in saturated water conditions (Hungr, Evans, Bovis, & Hutchinson, 2001). Iverson (2005) described debris flows as an intermediate event between dry rock avalanches and sediment-laden water floods whose distinction must be based on a strong interaction between solids and liquids. Later, Jakob and Hungr (2005) emphasized that the term *debris flow* should be used to represent the whole process, since an initiation slide in a slope, the extremely rapid flow along a steep confined channel, and the deposition on a debris fan. Also, the material classification was adapted according to geomorphological conditions, giving place to other terms such as mud flow, debris flood, and debris avalanche.

Nevertheless, differentiating between these phenomena, especially debris floods and debris flows, is difficult since the sediment concentrations can vary considerably across space and time. Thus, distinctions based on the peak discharges are often found in the literature. For instance, while debris floods have peak discharges limited to two or three times a major flood, debris flows may have extremely large peak discharges around fifty times more than a major flood (Jakob & Hungr, 2005). The differences in the discharges are directly related to the destructive power. Also, there are hydro-geomorphological differences in both processes. A debris flood is generated when the erosion power of a stream drastically increases due to highly intense rainfalls, landslide dams, man-made dams, or glacial lake outbreaks producing extreme floods or flash floods (Borga, Stoffel, Marchi, Marra, & Jakob, 2014). In these scenarios of extreme floods, the stream bed may be destabilized, causing a significant movement of sediments through rolling and saltation, which is called debris flood (Hungr et al., 2014). On the other hand, the same rainfall event may trigger clusters of landslides, whose deposits may reach the flooded channel. The sediment concentration increases to the point where the mix of water/sediments becomes a debris flow.

For mud flows, Hungr et al. (2014) suggested that the difference is given by the proportion of fine-grained material reflected in the plasticity. In that way, mud flows have much higher plasticity indices in comparison to debris flows. Lastly, in the case of debris avalanches, the primary distinction is that they can be found anywhere on steep slopes without entering into an established channel. However, it is common for debris avalanches to enter into pre-defined channels and become debris flows (Hungr et al., 2014).

In the Colombian context, this large group of phenomena is technically referred to as *avenidas torrenciales*. During this research, the term is further addressed as *torrential flows*.

2.2. Susceptibility and hazard models

Torrential flows are commonly modeled with approaches focused on the susceptibility and hazard of slope stability (source areas), which can be either qualitative or quantitative (Reichenbach, Rossi, Malamud, Mihir, & Guzzetti, 2018). The models used in the literature can be grouped into three prominent families, as shown in Table 1.

In the heuristic/knowledge-based models, the outcomes are primarily determined by the knowledge/skills of an expert. These methods are often applied when there are no sufficient data available to account for other modeling approaches. Besides, the main benefit is that the expert's knowledge can be incorporated, which allows establishing relationships that are difficult to estimate when analyzing only the data. Frequently, photointerpretation and fieldwork campaigns are carried out to support the execution of these approaches. They may vary from direct methods, such as detailed geomorphological maps and process inventory analysis, to indirect methods like multi-criteria assessment, where the expert ranks different variables associated with the phenomena of interest (Castellanos Abella & Westen, 2007).

Table 1. Examples of the different sets of techniques to evaluate landslide susceptibility and hazard.

Type	Group	Method	Examples	
Qualitative	Heuristic	Geomorphological mapping	(Westen, Rengers, & Soeters, 2003)	
		Inventory analysis	(Galli, Ardizzone, Cardinali, Guzzetti, & Reichenbach, 2008)	
		Multi-criteria decision analysis	(Bahrami, Hassani, & Maghsoudi, 2020; Meena, Mishra, & Piralilou, 2019)	
Quantitative	Physically-based	Iterative slope failure	OpenLISEM (Bout, Lombardo, Westen, & Jetten, 2018a)	
		Infinite slope	TRIGRS (Saadatkhah et al., 2016)	
		Random spheroid sampling	SCOOPS 3D (Palazzolo et al., 2021)	
		Finite slope based	Slide-rocscience (Khan & Wang, 2021)	
		Index of entropy	(Constantin et al., 2010)	
	Data-driven	Statistical	Weights of evidence	(Westen et al., 2003)
			Frequency ratio	(Chen et al., 2017)
			Information value	(Lin et al., 2004)
			Logistic regression	(Lombardo et al., 2018; Steger et al., 2016)
			Discriminant analysis	(Murillo-García et al., 2015)
Machine learning	Machine learning	Support vector machine	(Ballabio & Sterlacchini, 2012)	
		Random forest	(Barbosa et al., 2021)	
		Artificial neural networks	(Ermini et al., 2005)	

Physically-based approaches describe instability through mechanical laws. Hence, they consider the materials' rheology and their interaction with external and internal settings. These methods account for slopes failures and the estimation of failure volume and timing, which results in hazard estimations (Bout et al., 2018). Its applicability is often restricted to small areas due to the computational time and the highly detailed information (geotechnical data) needed to conduct these analyses. Recently, the inclusion of slope stability models couple with full hydrological models allows accounting for multi-hazard events.

Data-driven methods are built under the fundamental assumption that future landslides will be more likely to occur under environmental settings associated with the past or present landslide (Guzzetti, 2006). These approaches study the functional relationships between the presences/absences provided in a landslide inventory over a set of known predisposing and triggering factors. Moreover, the gain relies on their applicability in large areas since they do not require specific pre-defined information at specific resolutions. The landslide susceptibility literature tends to establish distinctions between statistical-based and machine learning methods within the data-driven methods. In terms of the use, the difference is that while statistical models go more towards the understanding and interpretation of predisposing factors, machine learning leans towards the performance of predictions because of their 'black box' nature (Goetz, Brenning, Petschko, & Leopold, 2015).

2.3. Generalized Additive Models (GAMs)

In a general context, a Generalized Linear Model (GLM) was firstly introduced by Nelder and Wedderburn (1972) as a flexible generalization of an ordinary linear regression under the assumption that the errors in the response do not strictly need to follow a normal distribution. For example, GLM can handle Poisson, Binomial, Bernoulli, among other distributions. In the geomorphological literature, GLMs are one of the most common statistical approaches (Brenning, 2005). They are implemented with a logit function (logistic regression), which allows handling a binary response, e.g., presence/absence of landslides. A GLM can establish linear relationships between dependent, continuous/discrete variables and an independent binary (in this case) response.

$$\text{logit}(P) = \beta_0 + \beta_1 X_1 + \dots + \beta_n X_n \quad (1)$$

Equation (1) illustrates the general structure of the GLM with a logit link (logistic regression) function in a landslide susceptibility context. P is the landslide susceptibility, β_0 refers to the global intercept and $\beta_n X_n$ refers to the regression coefficient β_n associated to each one of the covariates X_n .

Furthermore, a GAM can be understood as a non-linear extension of a GLM. Unknown smooth functions are added into the GLM structure (Equation (2)) to model non-linear associations between the predictors and the binary response. Also, fixed (linear) and random (non-linear) effects can be modeled with GAMs. For the particular case of random effects, the variables can be modeled as *iid* (independent and identically distributed) or using a random walk option of the first order (*RW1*) (Bakka et al., 2018). The primary difference is that *iid* treats the classes of a discrete covariate as independent from the other classes. Meanwhile, *RW1* accounts for dependency among the classes of an ordinal covariate. GAMs are well known for landslide susceptibility because of their high performances and the transparent interpretation of the results (Brenning, 2005).

$$\text{logit}(P) = \beta_0 + \beta_1 f_1(X_1) + \dots + \beta_n f_n(X_n) \quad (2)$$

Equation (2) shows the structure of a GAM with a logit link (logistic regression). The terminology is the same as describe in Equation (1). The difference is the term f_n which refers to the unknown smooth function associated to each one of the covariates X_n .

The GAM models are implemented in a Bayesian framework through INLA. As mentioned before, INLA is a novel approach that makes Bayesian inference faster (Rue et al., 2009) and can be implemented through the R package R-INLA.

3. STUDY AREA

This chapter focuses on (1) the physiographical description of the study area, (2) geological and tectonic context, and (3) administrative context regarding the urban planning regulations for torrential flows.

3.1. Location

The territory of the Republic of Colombia is located in the northwestern corner of South America (see Figure 1). Colombia is crossed from south to north by the Andes Mountain range. The Colombian Andes is divided into three ranges (east, central, and west), and intermediate valley lowlands with elevation ranges from 0 to ~5000 m asl in the most prominent zones. Moreover, the subduction of the Nazca and the Caribbean underneath the South American plates creates an active tectonic setting with regional fault systems, which results in a significant number of earthquakes with different magnitudes and depths and severely fractured lithological units (Pulido, 2003). Also, a series of active volcanoes, some of which are snow covered, provide an additional initiation mechanism for torrential flows (e.g., the lahars that destroyed Armero in 1985). Besides, because of its equatorial position, where the climate is mainly controlled by the Intertropical Convergence Zone, Colombia experiences intense rainfalls influenced by the atmospheric circulation over the Atlantic and Pacific oceans combined with the Amazon and Orinoco basins (Poveda et al., 2007). This combination of environmental settings produced a geomorphologically dynamic landscape with a significant concentration of mass movements and other erosive processes.

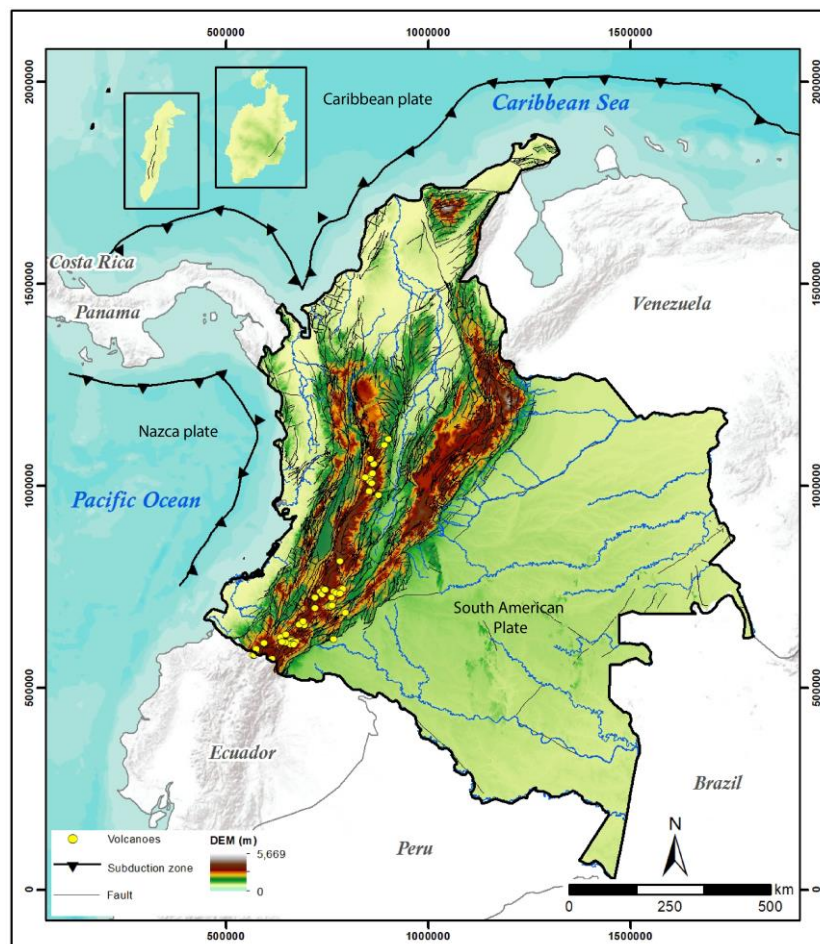


Figure 1. Location and physiographical overview of Colombia..

3.2. Geomorphological and geological settings

The geological settings of Colombia are very diverse, with lithological units of many types and ages ranging from the Paleoproterozoic to the Holocene (Gómez Tapias et al., 2020). In the Colombian Andes, each of the three mountain ranges has a different geological composition. For example, the Western range (Cordillera Occidental) has a volcanic/volcanoclastic origin evidenced by the presence of basalts, gabbros, and Late Cretaceous sedimentary rocks. The middle-range (Cordillera Central) is more characterized by a low-grade metamorphic Triassic basement with plutonic intrusions and volcanic rocks produced by the subduction of the Nazca under the South American plate. Finally, the Eastern range (Cordillera Oriental) consists of a high-grade metamorphic basement followed by thick successions of Cretaceous marine and continental sedimentary rocks (Gómez Tapias et al., 2020).

Towards the north coast, the Caribbean region is dominated by Triassic and Cretaceous marine and Jurassic continental sedimentary rocks with some Jurassic plutons in most of the Sierra Nevada de Santa Marta (Cardona et al., 2010). It is also remarkable the presence of Paleogene sedimentary rocks and significant extensions of Quaternary alluvial deposits. On the other hand, the Pacific coast in the west is mainly composed of cretaceous basalts and volcanoclastic sequences derived from an island arc accreted to the continental margin. (Gómez Tapias et al., 2020).

The largest regions (~50% of the country) are located on the east side and consist of the Amazon and Orinoco basins. A Paleoproterozoic basement characterizes these regions with Mesoproterozoic granitic intrusions, which form part of the Guiana shield. Finally, the insular regions in the Caribbean are composed of Pleistocene limestone rocks and alkaline Miocene volcanic rocks (Castillo & Vargas, 2013).

Carvajal-Perico (2012) proposed a framework to standardize the geomorphological cartography in Colombia. This framework establishes an entire hierarchy to account for the systematic classification and analysis of geofoms efficiently. The first level of the hierarchy (scales 1:2,500,000) is the geomorphostructures (GMS). This category refers to broad continental spaces characterized by regional geological structures and where the rocks have suffered deformation, metamorphism, or igneous intrusions. Plateaus, extensive sedimentary basins, rift valleys, and orogenic belts are some examples of GMSs. Furthermore, the GMSs are further divided into geomorphological provinces (scales 1:1,000,000). The provinces consist of groups of regions with similar geofoms that exhibit a similar geological genesis. For instance, mountainous belts, peneplains, and continental platforms, as Figure 2 shows.

The region of interest is defined based on the geomorphological map. The peneplains, the Guiana shield, the cratonic plateau are not included in the analysis. In other words, the east side of the country is excluded because it corresponds to the extensive Amazonian and Orinoquia flatlands, where due to their geomorphological conditions, the processes are flooding-type rather than torrential flow type.

3.3. Administrative context

With a continental area of almost 1.2 million km², Colombia is administratively divided into 32 departments and further divided into 1,128 municipalities. Each municipality's responsibility is to formulate its Land Use Plan (in Spanish Plan de Ordenamiento Territorial or POT) every 12 years. The POTs are technical tools to manage urban planning at municipal scales. The land-use planning policies state that hazards assessments for landslides, floods, and torrential flows are basic information requirements within the POT frame.

The land use regulation establishes two levels of hazards assessments at different scales. The first one corresponds to the basic hazard studies. In these studies, the landslides, floods, and torrential flows hazard

must be evaluated at scales 1:25,000 and 1:5,000 for rural and urban/urban expansion areas, respectively. Thereby, areas under hazardous conditions, consisting of un-populated areas classified with a high or medium hazard level, are mapped. Areas under risky conditions, i.e., populated areas classified as high hazard, are as well delimited. Consequently, detailed hazard studies must be conducted whenever a municipality plans to develop or grow in areas under risky or hazardous conditions. The scales for the detailed studies are 1:5,000 and 1:2,000 for rural and urban/urban expansion areas, respectively. Based on these results, mitigation measures must be included as part of the POT.

Standard landslide and flood guidelines for hazard assessment in Colombia have been clearly described by SGC (2015) and IDEAM (2017), respectively. However, there had not been any consensus regarding standard methods for the hazard assessment of torrential flows. In recent years, the SGC, in association with Pontificia Universidad Javeriana (PUJ), started building the guidelines for torrential flow hazards, which are not finalized yet (SGC & PUJ, 2020).

The proposed methodology consists of two stages. In the first stage, a hazard assessment at a scale of 1:25,000 is conducted. First, the Digital Elevation Model (ALOS PALSAR 12.5) must be topographically corrected using road intersections, ground control points, and drainages. This is proposed as an alternative for obtaining a fair cartographic representation for the torrential flows, given that most of the municipalities do not count with detailed cartographic products. Then, based on the corrected DEM, the municipality is divided into watersheds. Each watershed needs to be individually characterized in terms of torrentiality. This is done through detailed geomorphological mapping of torrential deposits and the compilation of historical torrential flow records. Afterward, rainfall return periods are established based on a statistical analysis of the national rain gauge network or local rain gauges. If there are no rain gauges in the proximities, satellite rainfall data can be considered an alternative. The considered return periods are 2.33, 5, 10, 25, 50, 100, 300 and 500 years (SGC & PUJ, 2020).

The initiation process for every watershed in the municipality is assessed using empirical hydrological models; besides, the solid volume is calculated based on geometric and geological factors. Geotechnical properties of the materials and physically-based methods are always suggested whenever the information is available. The transport and deposition processes are carried out using runoff models such as Flod-2D, RAMMS, RiverFlow2D, and TITAN2D. As a result, the maximum flow depths and velocities for each return period are obtained and combined in integration matrices to calculate the hazard level.

The second analysis stage at a 1:2,000 scale focuses on medium and high hazard areas classified by the 1:25,000-scale assessment. The proposed physically-based methods involve highly detailed information, such as granulometry, friction angles, cohesion, densities that need to be sampled at the determined watersheds. Unlike at the previous scale, the detailed assessment includes the calculation of sediments produced from the lateral erosion of the channel by using physically-based slope stability models. The recommended physically-based models are r.avafLOW, D-Claw iRIC, among others. The hazard classification is based on the flow intensity index and the determination of its exceedance probability.

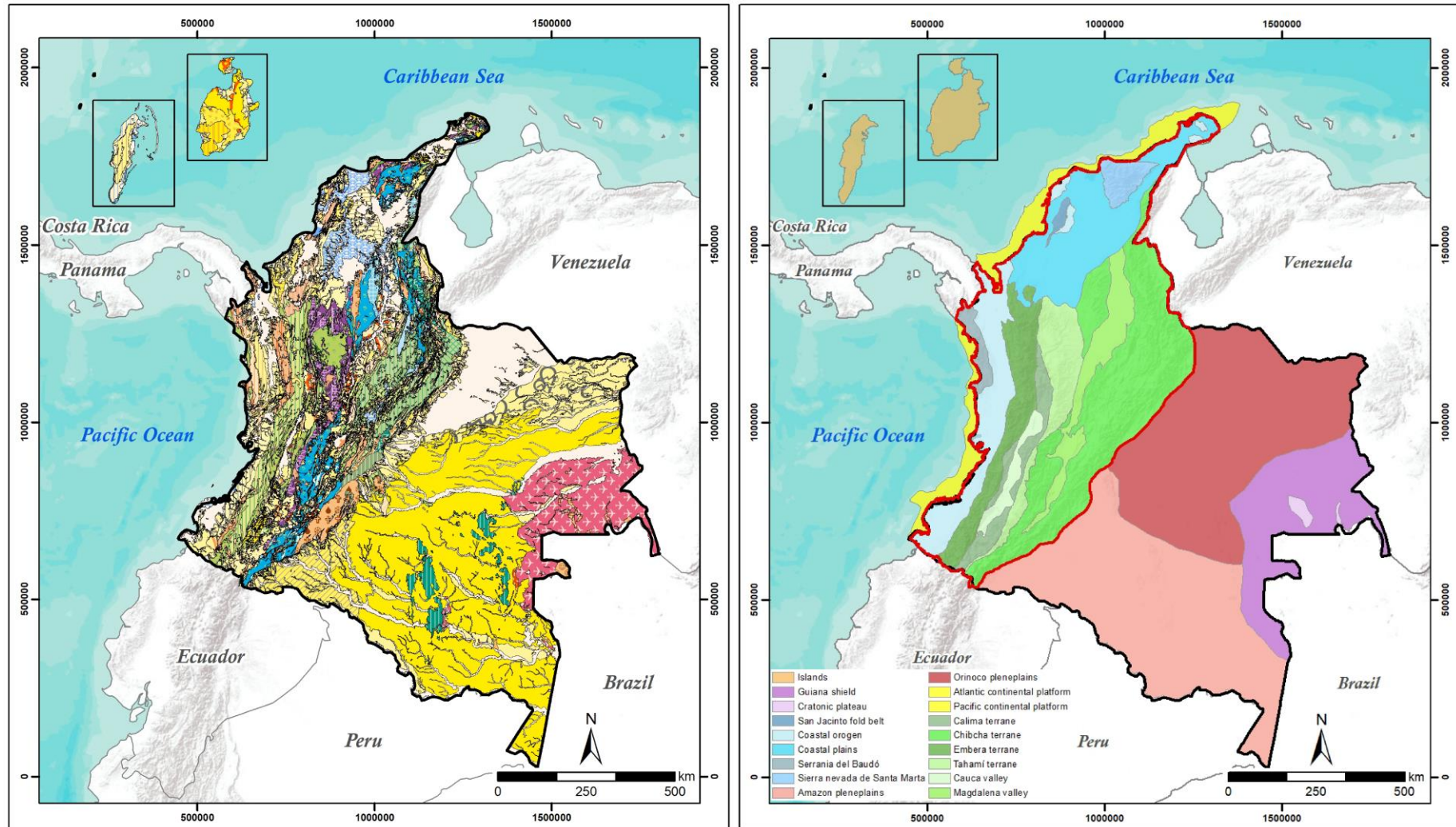


Figure 2. On the left side, the geological map of Colombia at a scale 1:1,000,000. The colors follow the International Chronostratigraphic Chart, and the detailed map and legend are available in the interactive application provided by [SGC](#). On the right side, the geomorphological provinces describe by Carvajal-Perico (2012). The boundary in red corresponds to the region of interest.

4. DATA

This chapters depicts data collection and preprocessing for (1) the inventories, (2) the digital elevation model, (3) the thematic predisposing factors, (4) the triggering factor, (5) the cartographic database and (6) the reference level watersheds.

This research uses and integrates data from multiples sources (see Table 2). All data are freely available and can be retrieved through web resources. Besides, all data were handled in official cartographic reference system MAGNA-SIRGAS/Colombia Bogota ZOne - EPSG:3116. Below, an overview of the data sources and ata preparations is given.

Table 2. Summary of the different datasets used during this research. The symbol (-) indicates that the information was not available and therefore could not be retrieved.

Dataset	Resolution	Geometry	Source		Purpose
SRTM	90m x 90m	Raster TIFF	The National Aeronautics and Space Administration	NASA	Terrain derivatives
Lithology	1:1,000,000	Vector polygon	Servicio Geológico Colombiano	SGC	Static predisposing factor
Land cover	1:100,000	Vector polygon	Instituto de Hidrología, Meteorología y Estudios Ambientales	IDEAM	Semi-static predisposing factor
Land use	1:100,000	Vector polygon	Instituto Geográfico Agustín Codazzi	IGAC	Semi-static predisposing factor
Rainfall	5 km x 5 km	Raster TIFF	Climate Hazard Center, UC Santa Barbara	CHIRPS	Triggering factor
Cartographic base	1:100,000	Vector point/polyline/polygon	Instituto Geográfico Agustín Codazzi	IGAC	Prioritization of areas
Watershed	N.A.	Vector polygon	Instituto de Hidrología, Meteorología y Estudios Ambientales	IDEAM	Reference level for watershed delineation
SIMMA inventory	N.A.	Vector point	Servicio Geológico Colombiano	SIMMA	Susceptibility model
DesInventar inventory	N.A.	Vector point	United Nations Office for Disaster Risk Reduction	DesInventar	Susceptibility model

4.1. Inventory

Three different point-based inventories were applied to model the torrential flow susceptibility.

4.1.1. SIMMA

The Sistema de Información de Movimientos en Masa (SIMMA, <http://simma.sgc.gov.co/>) is a web system supported by the SGC that allows loading, storing, searching, and downloading records of mass

movements in Colombia. Also, it gives access to reports, projects, and information regarding studies for landslide susceptibility and hazard carried out by the Geohazard division in the SGC. Each record is represented geometrically as a point and classified into slide, flow, rockfall, toppling, and creeping. From the SIMMA platform, two main products can be obtained:

- Catalog (3,425 events): It is a database of mass movement historical records obtained from secondary sources such as the news, Red Cross reports, and Civil Defense. Despite the uncertainty limitations, this product gives an overall understanding of the qualitative and quantitative impacts of landslides. Every event contains a limited number of attributes in which for this research, it is essential to highlight the coordinates, status, type, subtype, deaths/injured people, uncertainty, economic damage, and environmental damage. In this study, only events with low uncertainty were considered for susceptibility modeling.

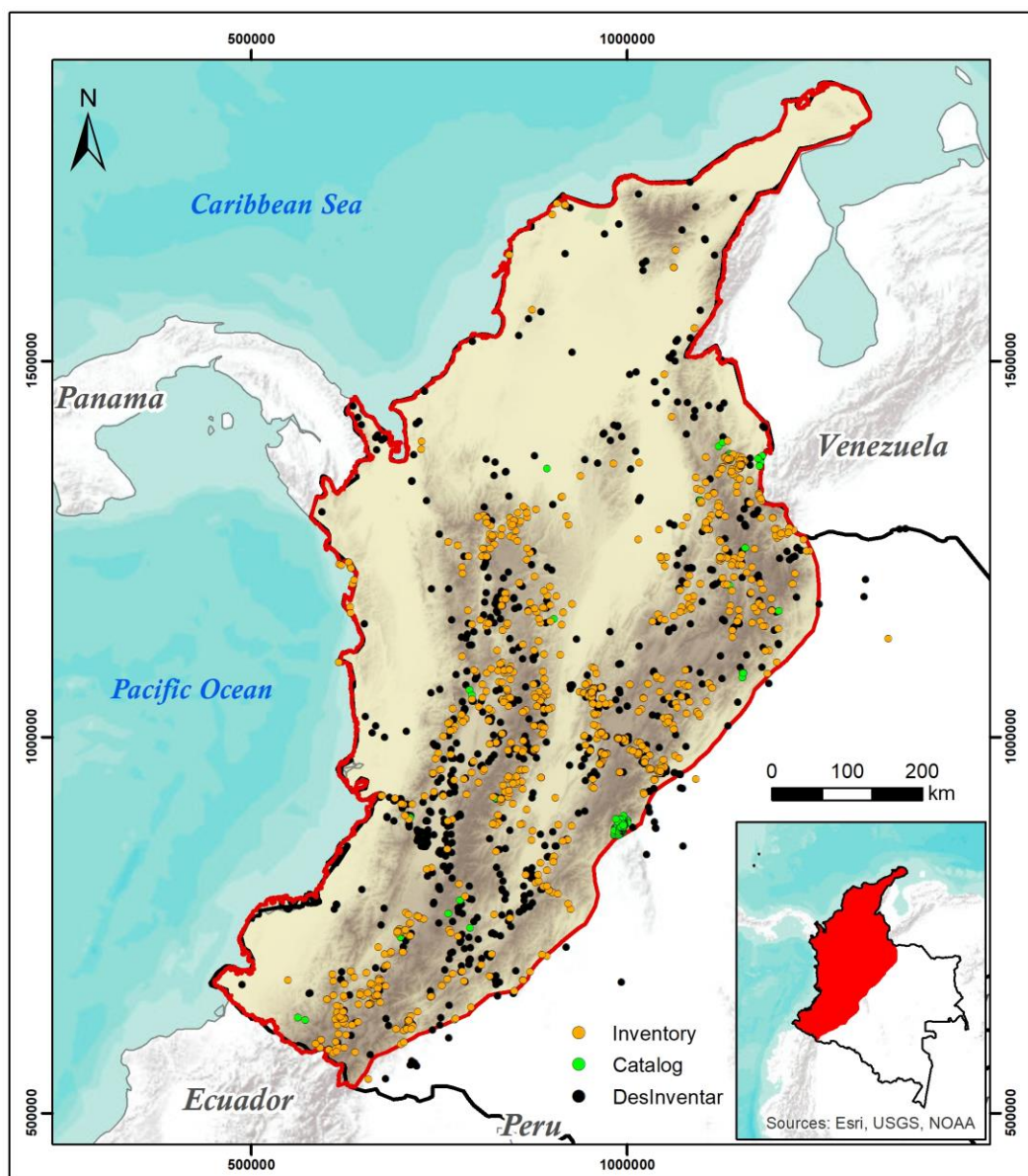


Figure 3. Location of the study area showing the three considered inventories and the region of interest (red boundary) based on the proposed standardization for the geomorphological cartography in Colombia.

- Geomorphological inventory (1,086 events): This type of inventory is based on geomorphological interpretation and digital imagery processing supported by fieldwork. It combines historical records and event-based records, which refer to the landslides related to a specific triggering event, e.g., a rainfall event or an earthquake (Guzzetti et al., 2012). Compared to the catalog, this product has a much more complete description and classification of the events. In fact, since the mapping of the events is supported by fieldwork, low uncertainties may be reasonably assumed.

4.1.2. DesInventar

The Sistema de Inventario de Desastres (DesInventar, <https://www.desinventar.net/>) is a tool for the generation and standardization of national disaster inventories focusing on the different types of losses and impacts due to disasters. DesInventar in Colombia was initially developed by La Red de Estudios Sociales en Prevención de Desastres (LA RED), Corporación Observatorio Sismológico del Suroccidente Colombiano (OSSO) and United Nations Office for Disaster Risk Reduction (UNISDR).

DesInventar contains records (1,363 events) of small, medium, and greater impact by torrential flows based on pre-existing data, newspapers, academic studies, and institutional records. Important attributes relate to the number of casualties, injuries, destroyed houses, damaged houses, etc. However, there is no information regarding the type of torrential flow. Moreover, the data do not have a spatial location or coordinates but descriptions of the potential locations. To overcome this issue, every single event was manually georeferenced based on the description provided in the inventory. The location of events (point-based) was supported by Google Earth, and land use features taken from the official cartographic database of Colombia.

For the georeferentiation, since the location of the events does not follow any systematic description (i.e., poor, or detailed descriptions of the locations were found), an indicator to measure the uncertainty of location was used as shown in Table 3.

Table 3. Uncertainty level estimation for the spatial location of the DesInventar inventory.

Uncertainty level	Meaning	Number of torrential flows
N.A.	It contains location errors. For example, the river/stream where the event occurred is not located in the stated municipality. In some cases, the mentioned municipality is not even in the stated department.	2
Very high	The stated location is not specific at all, e.g., only the municipality's name is mentioned in the description.	433
High	Very few reference elements are described. For instance, description of events based on small mine's name that can be hardly found or may not exist nowadays. (Common for events prior 2000)	97
Moderate	Broad description with almost no reference elements, i.e., only the municipality and the name of the river/stream are described.	106
Low	Good description with some basic reference elements such as the municipality, the river/stream, veredas, and affected areas.	193

Very low	The description is well done with plenty of details of reference elements. For example, the municipality, the river/stream, the affected area, and other elements such as relative location to school, hospital, police stations, and bridges are clearly described.	591
-----------------	--	-----

For further analysis, the Catalog and Inventory from SIMMA were combined and treated as single SIMMA since, in principle, they refer to the torrential flow source areas. On the other hand, DesInventar remains as an independent inventory since it depicts the areas impacted by torrential flows. Table 4 indicates the distribution of events according to the three processed inventories. Recall that only events with low uncertainties are considered for further analysis. Figure 4 shows an example of how SIMMA (in white) tends to be located toward the mountainous areas and DesInventar toward the flatlands.

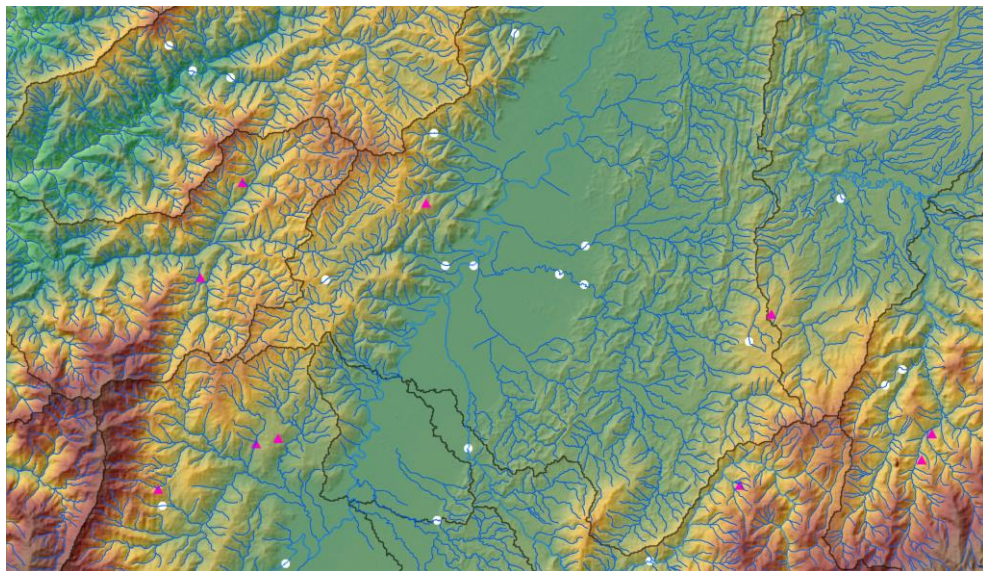


Figure 4. Visual comparison between SIMMA (magenta triangles) and DesInventar (white dots)

Table 4. Summary of the used inventories according to the type of torrential flow. The numbers shown correspond to the filtered data (by uncertainty) used for the susceptibility model.

Type of event	Catalog - SIMAA	Inventory - SIMMA	DesInventar
Debris flow	16	467	*
Debris flood	4	249	*
Mudflow	21	256	*
NULL	317	114	*
Total	358	1,086	784

* Note that DesInventar does not contain information regarding the classification of the event. All the events are classified as torrential flows.

4.2. Digital Elevation Model (DEM)

DEMs are essential input data since it allows deriving important terrain and morphometric features of an area. The Shuttle Radar Topography Mission (SRTM) is a digital elevation dataset that provides high-quality elevation data for over 80% of the globe (Farr et al., 2007). For this thesis, the main product

considered is the SRTM Digital Elevation Data Version 4 3 Arc-Second. This version of the SRTM digital elevation (90m cell size) data has been processed to fill voids and facilitate its use. The data were searched, clipped, and download through the geospatial processing service Google Earth Engine (GEE). Terrain derivatives such as slope, relief, curvatures, and topographic wetness index were generated from the DEM for further analysis (The code can be found in the Appendix 10.6)

4.3. Thematic predisposing factors

The set of environmental predisposing and triggering factors is composed of data regarding the geological, land cover, land use, and rainfall conditions: Other predisposing factors, i.e., the morphometric indices, are introduced later on.

4.3.1. Lithology

It consists of the geological and structural information of Colombia at a scale of 1:1,000,000. For its design, previous 1:100,000 scale geological maps issued by SGC were integrated into a single cartographic product. The harmonization was controlled using Landsat T.M, radar imagery, and the relief map produced with a 30-m-resolution DEM.

The geological units were defined according to a chronostratigraphic classification system and grouped by age and material type. The age classification followed the International Chronostratigraphic Chart 2020. Rocks and deposits were the primary division in terms of material. Moreover, rocks were subdivided following the rock type, i.e., igneous, sedimentary, metamorphic, and volcanoclastic. These subdivisions were further divided until they reached the rock-name level, i.e., granites, marbles, and conglomerates. On the other hand, deposits were grouped according to their geomorphological environment, e.g., alluvial, alluvial fan, alluvial terraces, paludal, glacial, coastal, and eolean and volcanic ahh deposits. Faults, folds, and other structural attributes are also included in this dataset.

To ensure an adequate interpretation and reduce the complexity of the model results, it was necessary to decrease the number of classes in the geological map. Twenty-five base classes were proposed to describe each lithological unit. The proposed base classes are the generic rock types that are used to disaggregate or parametrize the geological units. Table 5 depicts examples of the parametrization process. As a result, the original 279 classes in the geological map are translated into 25 base classes, later used as static predisposing factors in the susceptibility model.

Table 5. Example of the disaggregation procedure for the lithological map. On the left side, the original lithological units, on the top, eight of the twenty-five base classes. 1/0 is used to represent the presence/absence of the base class in the respective lithological unit.

Original lithological unit	Conglomerate	Sandstone	Claystone	Coal	Basalt	Andesite	Schist	Amphibolite
Conglomeratic sandstones, sandstones, claystones and coal	1	1	1	1	0	0	0	0
Basalts and andesites	0	0	0	0	1	1	0	0

Quartz schist and amphibolite with garnets	0	0	0	0	0	0	1	1
Basalts, andesites, claystones and sandstones	0	1	1	0	1	1	0	0

The final twenty-five lithological classes are surface deposit, conglomerate, sandstone, siltstone, claystone, mudstone, shale, coal, limestone, rhyolite, andesite, basalt, granite, diorite, gabbro, peridotite, breccias, tuff, serpentinite, phyllite, schist, quartzite, marble, amphibolite, and gneiss. Since the complete tables in which the disaggregation was done, were too long to be included even in the appendix, they were not reported.

4.3.2. Land cover

This cartographic product was developed by IDEAM using an adaptation of the CORINE Land Cover methodology for Colombia. The map describes land cover features (up to level 3) derived from mid resolution (30 m) Landsat 5 and Landsat 7 for the period 2010-2012 (IDEAM, 2010). In some areas, due to clouds, SPOT, CBERS¹, and ASTER imagery were used to guarantee full coverage. The processing of the satellites images was carried out using semi-automatic classification techniques in GIS software. Also, depending on the complexity of the area, the classification was supported by manual delineation using aerial photos. As a final step and to check the quality control, fieldwork was conducted in specific areas selected according to their potential land cover diversity and the accessibility of the terrain.

The land cover map initially contained 60 different classes, so an aggregation process was done to reduce the complexity of the data and guarantee the interpretability of the results. Land cover classes were grouped according to their similarity with other classes and their potential relevance to torrential flows. Moreover, new class names and levels are proposed following the CORINE Land Cover methodology for Colombia developed by IDEAM (2010) to maintain consistency and coherence. Table 6 illustrates examples of the reclassification carried out. Consequently, the initial 60 classes were reduced to 23 new classes, as shown in Figure 5.

Table 6. Example of the reclassification for the land cover map. In the original level, the number of digits corresponds to the detail of the level. Therefore, three digits represent level 3.

Original class	Original level	New class	New level
Urban areas	111	Artificial surfaces	1
Airports	124		
Grassland	231	Grasslands	23
Grassland with bushes	232		
Grassland with trees	233		
Shrubby permanent croplands	222	Permanent croplands	22
Permanent crops with trees	223		

¹ China-Brazil Earth Resources Satellite program

Cereals	212		
Lakes and lagoons	512		
Artificial water bodies	514	Inland waters	41
Bushes	321	Shrub/herbaceous	
Shrubs	322	vegetation	32

A more detailed description of the reclassification can be found in Appendix 10.1.

4.3.3. Soil and potential Land use

IGAC in 2014 generated the soil map through fieldwork and laboratory analysis of different biophysical parameters such as climatic factors, geomorphology, type of material, soil wetness, soil depth, fertility, salinity content, and carbon content. Based on these parameters, the taxonomic classification of soils was carried out with national coverage. Despite the relevant information contained in the soil maps, they were not used during this research due to the lack of standardization. Each of the 32 departments in Colombia has soil maps with attributes that are not necessarily homogeneous among departments. Thus, the soil map had to be discarded due to the extensive clean-up process required for using the data.

In 2018, IGAC generated the map of potential land use for Colombia at a 1:100.000 scale. This product is derived from the national soil map issued in 2017. In line with the biophysical features previously described for the soil map, IGAC estimated indices to check land status. These indices quantify and distinguish the state of every land mapping unit, including their degree of deterioration. Besides, by analyzing these indices and soil potentialities, the primary potential land use was determined for each land mapping unit in the national territory. Since the original map soil could not be included in the analysis, the potential land use map, which can reflect features of the soil map is adopted instead. The potential strong relationships with the land cover map were later considered.

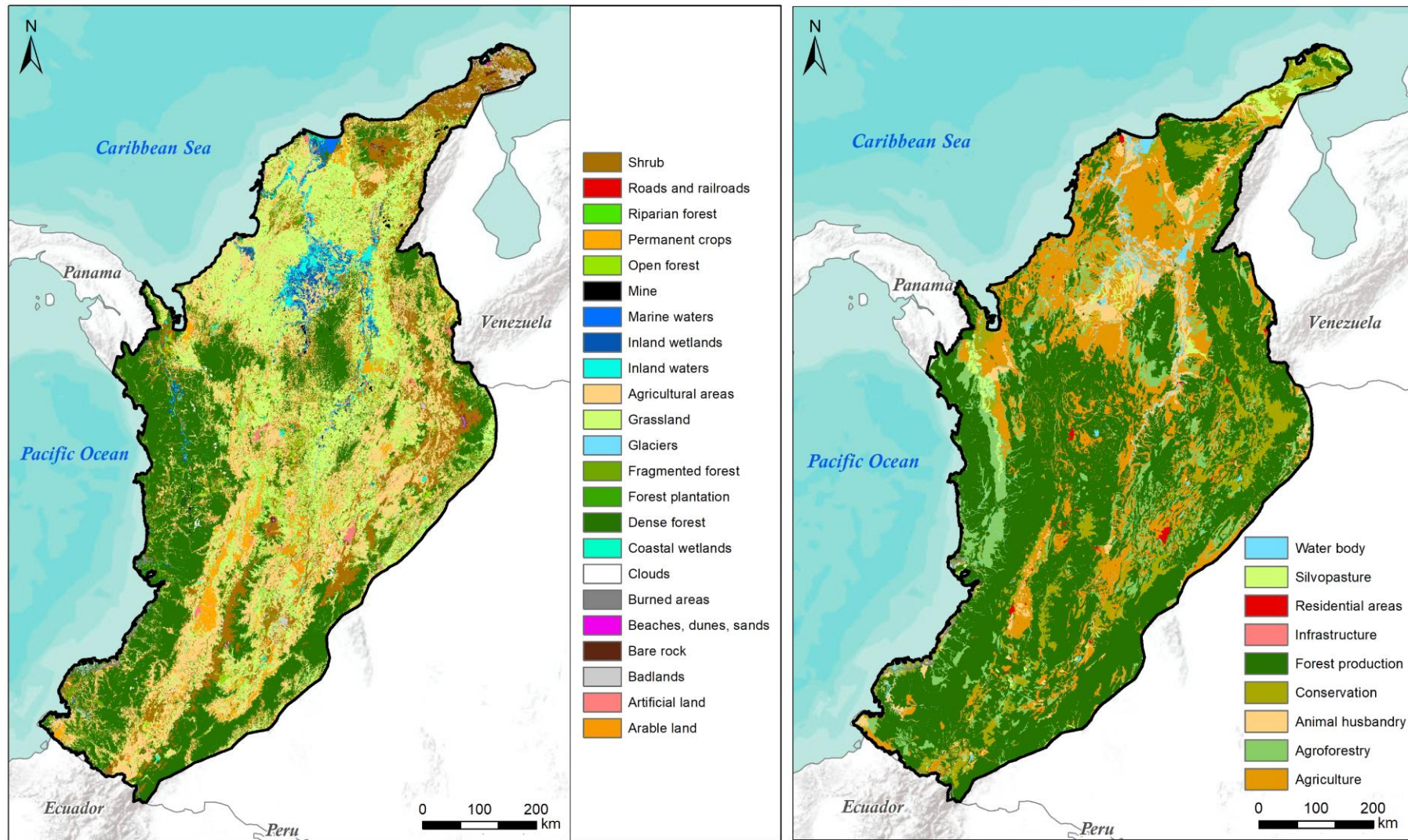


Figure 5. Land cover map (left side) and potential land use map (right side).

As in the land cover case, the potential land use map initially contained many classes that could lead to a misinterpretation of the model results. Hence, following the same idea (see Table 7) as for the land cover map, a reclassification is carried out to reduce the number of classes in the land use map. Consequently, the initial 48 classes are reduced to 9 new classes. Results can be seen in Figure 5.

Table 7. Example of the reclassification of the land use map.

Original class	New class
Semi-intensive permanent crops	Agriculture
Intensive permanent crops	
Extensive pasture areas	Animal husbandry
Intensive pasture areas	
Conservation of hydrological resources	Conservation
Conservation of hydrogeological resources	

The complete reclassification table is included in Appendix 10.2.

4.4. Triggering factors

4.4.1. Rainfall

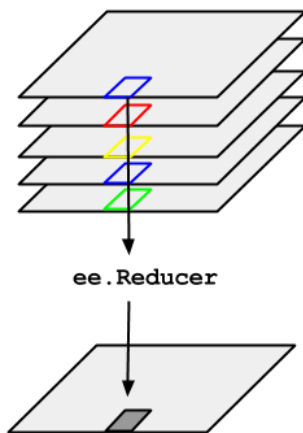


Figure 6. ImageCollection reduction functions (`ee.Reducer`) in GEE. Modified from <https://developers.google.com/earth-engine>.

Rainfall information was extracted from the Climate Hazards Group InfraRed Precipitation with Station data (CHIRPS). “CHIRPS is a +35-year quasi-global and high-resolution rainfall dataset that uses the Tropical Rainfall Measuring Mission Multi-satellite Precipitation Analysis version 7 to calibrate global Cold Cloud Duration rainfall estimates.” (Funk et al., 2015, p. 2). The dataset is considered quasi-global since it covers the area from 50°N to 50°S on a 0.05° grid (~5 x 5 km in the study area) at a daily temporal resolution. Comparing to other global or quasi-global satellite rainfall datasets such as TRMM² and GPM³, CHIRPS has information available for a more extended period. And, due to the scale of analysis (national scale), its spatial resolution represents and advantage when pre-processing the data.

The processing of the CHIRPS rainfall data for this study was handled in GEE. Since CHIRPS contains available rainfall data from January 1981 until December 2020, it is fundamental to consider aggregation methods through the temporal component. To achieve that, reducer functions (`ee.Reducer`) were applied in GEE. The reducer functions allow reducing an image collection to an individual image (see example in Figure 6) by applying statistical operations.

Resultantly, individual pixels contain the temporal aggregation using statistical descriptors, i.e., mean, median, min, and max estimated of all the images in the collection at that location. For the particular case of this research, rainfall was aggregated using the average and the maximum statistics. As a result, the average daily and maximum daily rainfall for each pixel in a time window from 1981 to 2020 were estimated in the entire study area.

² The Tropical Rainfall Measuring Mission

³ Global Precipitation Measurement

Another approach was implemented to capture the temporal variation of the precipitation in Colombia. For that, the daily rainfall was first aggregated into yearly rainfall, as Figure 7 shows. Then, for the period 1980-2020, the year with the maximum precipitation, 2011, was selected as a representation of an extreme precipitation scenario. Finally, for that particular year 2011, the total annual rainfall was computed for every pixel and later used it in the rainfall set for the susceptibility modeling.

An overview of the scripts used for the rainfall processing can be found in Appendix 10.3 and 10.4

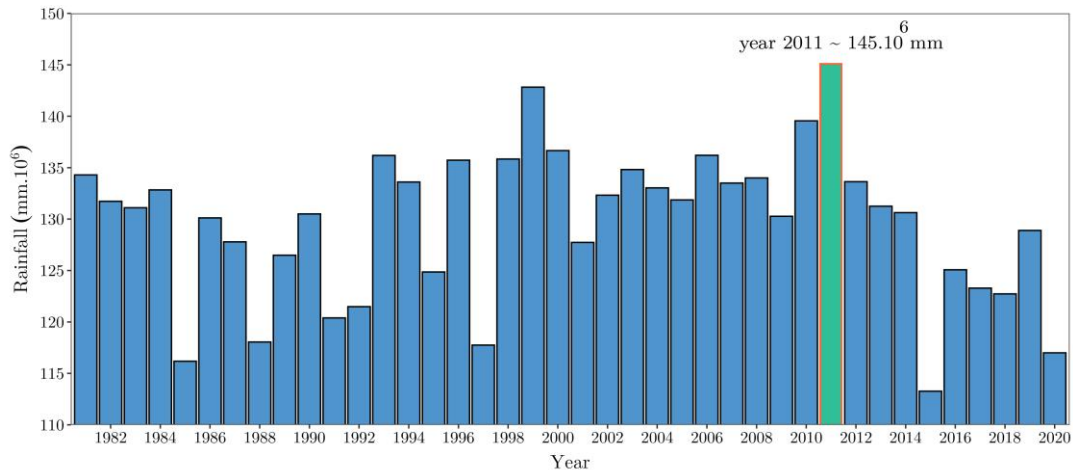


Figure 7. Total annual rainfall for a time window from 1980 to 2020. The bar in green represents the year with the maximum total annual precipitation.

4.5. Cartographic base

Instituto Geográfico Agustín Codazzi (IGAC) is the official institution responsible for producing the official and basic cartographic products in Colombia. IGAC has essential cartographic information at scale 1:100,000 and 1:500,000 at the national level freely available on their website. The data contain elevation curves, water bodies, drainages, artificial features such as roads, urban areas, etc. To generate these products, IGAC implemented the manual interpretation of aerial photos, optical and radar satellite images, i.e., Landsat, SPOT, RapidEye, TerraSAR-X, and GeoSAR, with fieldwork campaigns that have been doing since 1953. Furthermore, the database is under a continuous process of maintenance and update. Therefore, the information may have changes daily. For this research, information regarding the urban centers and the drainage network were considered.

4.6. Watersheds

The watersheds were extracted from the "Zoning and coding of hydrographic units and hydrogeological of Colombia" proposed by the Institute of Hydrology, Meteorology, and Environmental Studies (IDEAM, 2013). IDEAM proposed a hierarchical system that allows classifying Colombia according to its hydrographic characteristics. The entire country is divided into five main hydrographic areas, which are later subdivided into 316 catchments. These 316 subzones were assumed as the reference level for the mapping unit delimitation.

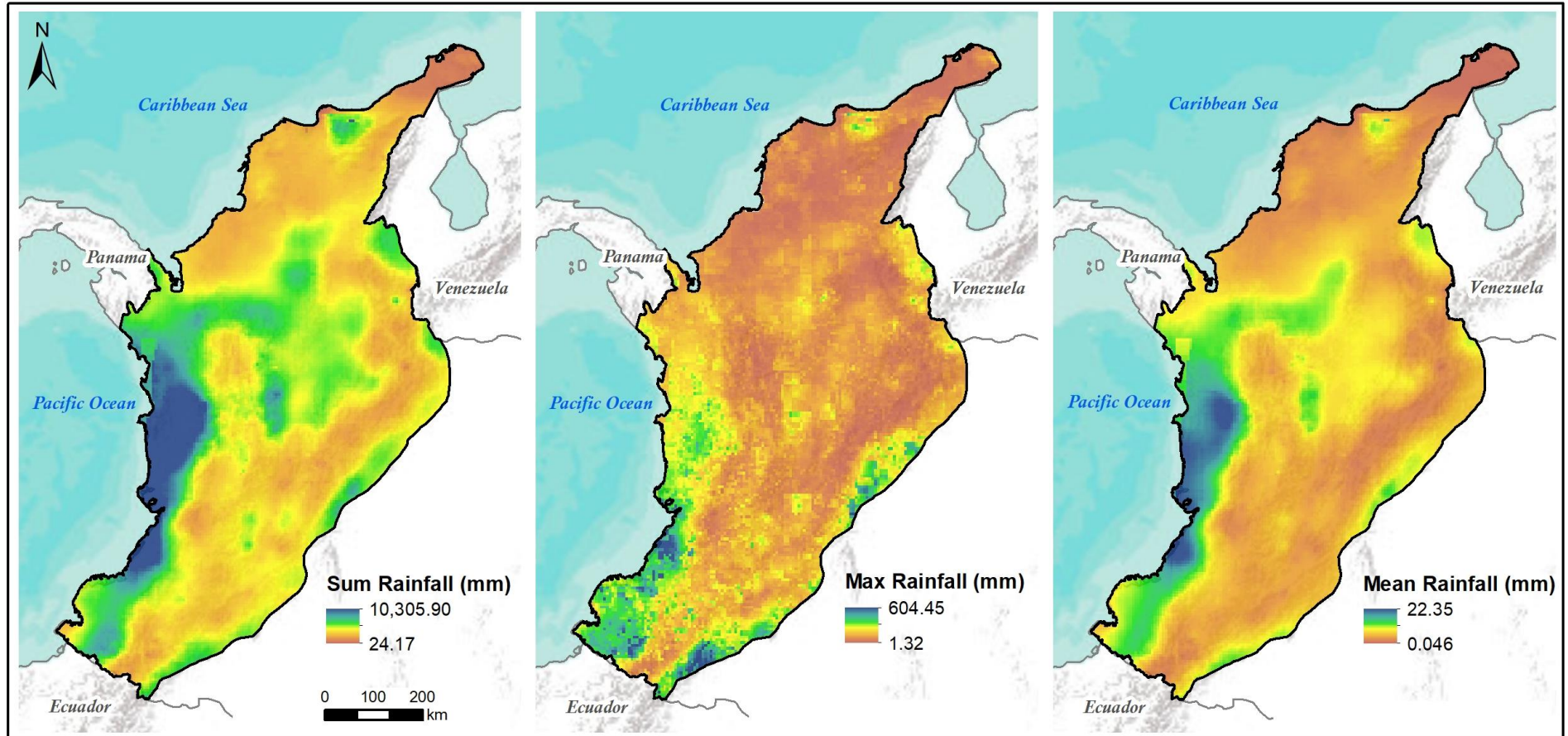


Figure 8. Temporal aggregation of the rainfall. From left to right, the total rainfall for the year with the maximum annual rainfall (2011), maximum daily rainfall, and mean daily rainfall.

5. METHODS

This chapter addresses considered methods for (1) watershed generation, (2) the role of the predisposing and triggering factors, (3) the selection of a suitable mapping unit to represent torrential flows and (4) the prioritization of watersheds according to the historical records, the susceptibility and the EaR.

Figure 9 illustrates the flowchart of the methods followed during this research. Firstly, as detailed in chapter 4, the data referring to the predisposing and triggering factors, and the inventories were generated and cleaned up. Secondly, morphometric indices were calculated using the DEM, the different levels of watersheds, and the stream network. These indices served as predictor variables together with the lithology, land cover, land use, and rainfall. The latter ones were also spatially aggregated in the watersheds, using the average, standard deviation, and proportions for the case of categorical covariates. Afterward, a multi-collinearity test was taken to ensure consistency and optimal interpretability of the covariate's effects. As a third step, exploratory models to account for the variable significance were implemented through R-INLA. Once the significant variables were selected, susceptibility and uncertainty were computed for the different mapping units. Results were validated using k-fold cross-validation and the respective Area Under the Receiver Operator Curve (AUROC). The final steps refer to the classification of the susceptibility map and the combination with the Elements at Risk (EaR) to prioritize areas prone to torrential flows.

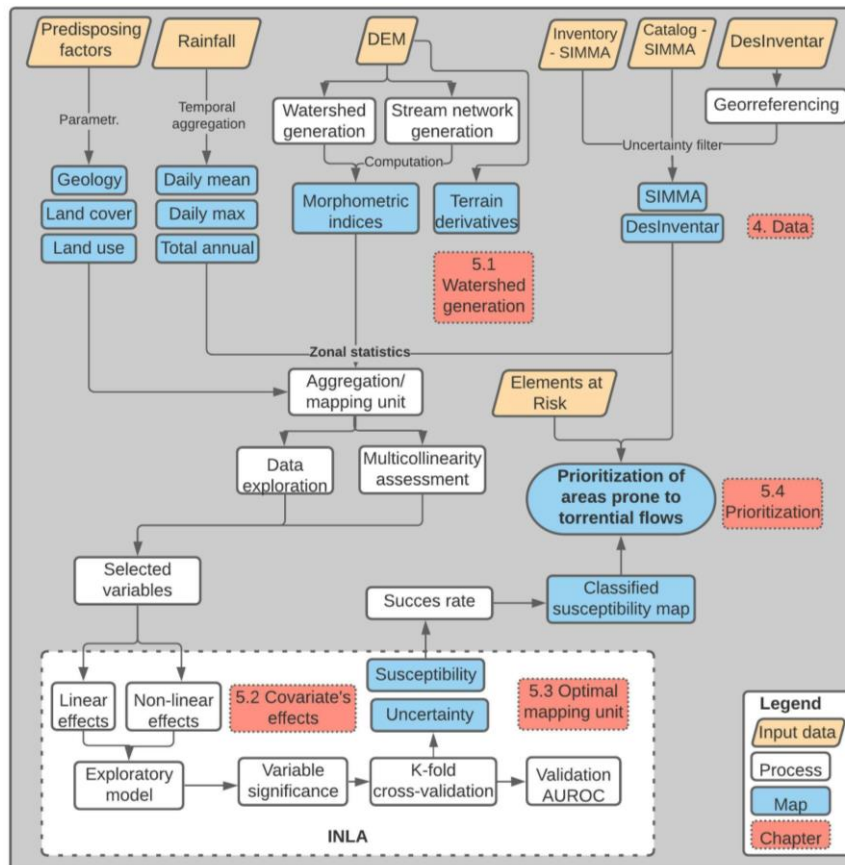


Figure 9. General overview of the methods.

5.1. Watershed generation

Choosing the basic unit mapping was crucial since it determined how the torrential flows were going to be represented, and how the descriptive variables were going to be aggregated (Rossi & Reichenbach, 2016). Reichenbach et al. (2018) found that pixels and slope units are the most common mapping units used for landslide susceptibility estimation in the geomorphological literature. However, an important characteristic of torrential flows is that the displaced material can travel from tens of meters up to several km along pre-existing channels. This creates the need to look at the process from a larger landscape partition, such as watersheds. Also, the use of watersheds can be seen as a way to integrate slope stability with transport and deposition processes since they all can take place in a watershed unit.

A watershed can be defined at several levels depending on the outlet point position. In other words, a watershed can be subdivided into sub-watersheds, and the sub-watershed can be further subdivided. For this analysis, five watershed levels were considered as mapping units in the susceptibility model. The five landscape partitions were assessed independently with the two torrential flow inventories to find a suitable representation for torrential flows.

5.2. Role of the predisposing and triggering factors in the occurrence of torrential flow events

5.2.1. Generation of morphometric indices

Once the mapping units were delineated, a new set of variables was computed. Several authors have identified the so-called morphometric parameters as good predictors to differentiate torrential from non-torrential watersheds (Welsh, 2007). These indicators indirectly give information about peak flow (see Figure 10) discharge, structural control of the watershed, potential infiltration, and sediment loss, as briefly explained in Table 8. According to the type of morphometric indices, they were grouped into areal features, linear, and topographic features. Then, the variables used for the susceptibility model were grouped into five categories: morphometric indices, lithology, land cover, land use, and rainfall. Terrain derivatives and rainfall were aggregated into the watershed through the average (μ) and standard deviation (σ). For the categorical variables, the proportion of each class within every watershed was calculated. That way, representative values were incorporated into the mapping units, in this case, the watersheds.

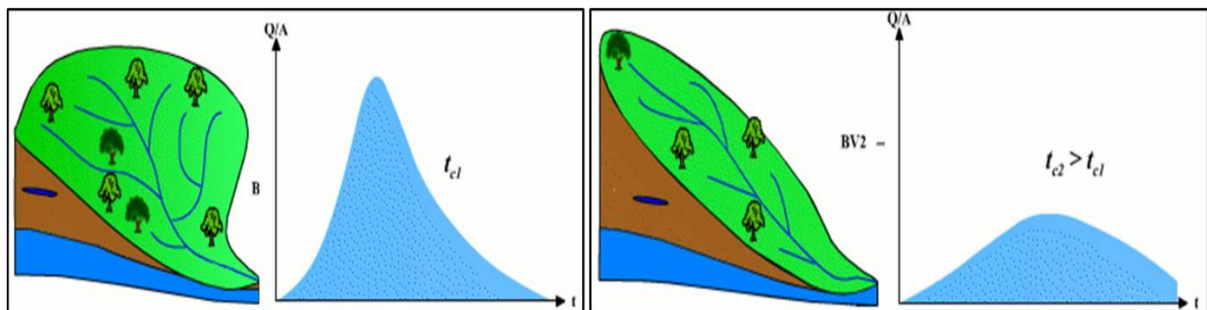


Figure 10. Influence of watershed geometry in the hydrograph. Modified of echo2.epfl.ch

5.2.2. Multi-collinearity test

The multi-collinearity analysis was carried out to avoid redundancy among the different sets of predisposing and triggering factors. Accounting for multi-collinearity becomes a critical step in the process since the results are highly influenced when there are strong relationships among the variables (Reichenbach et al., 2018). Consequently, this may potentially lead to misinterpretation of the predisposing factor significance, which is one of the goals of this research. Multi-collinearity was assessed using the

Pearson correlation coefficient, as known as Pearson's r . This metric does pair-wise comparisons for all the variables, determining a correlation coefficient for each pair of covariates. Pearson's r depicts strong relationships when its value is close to 1 or -1. Based on the results of this analysis, some variables were discarded. Moreover, the selection of these variables was not purely quantitative but also supported by a critical assessment of the information that the variable introduces to the model.

5.2.3. Covariate effects

Based on the region of interest size ($\sim 550.000 \text{ km}^2$), the available information, and this research's goals, GAMs were chosen as a framework to model torrential flow susceptibility. The two sets of inventories, SIMMA (further referred to as Mod1) and DesInventar (further referred to as Mod2), were independently modeled. All continuous variables were rescaled by subtracting their mean and dividing by their standard deviation. That way, the comparison among covariates is simplified since they are expressed on an equal unit-less scale.

The first step included the execution of exploratory models. The exploratory models used the total amount of data for training the GAM. Its purpose was to pre-screen the relationships between covariates-response and explore the gains and losses of modeling covariates as fixed or random effects.

The effects of the covariates were then determined by plotting their Regression Coefficients (RC). In the plot, the RC's magnitude and sign are used to draw the initial interpretation of the covariates. Also, the 95% Credible Intervals (CI) of the RC posterior distributions were calculated to assess the significance of the covariates.

Table 8. Summary of morphometrical indices included in the analysis. WL* stands for the watershed length. P* refers to the watershed perimeter. SN* is the number of streams. SL* stands for stream length. M stands for the average, and σ stands for the standard deviation.

Group	Factor	Estimation	Importance	Reference
Areal	Watershed area (A)	A	The wider the watershed, the larger the amount of water it can collect, diluting the flood and reducing the chance of having torrential flows.	(Schumm, 1956)
	Form factor (F)	$F = A/WL^*$	It relates to the flow peak discharge and the debris flow occurrence.	(Wohl et al., 1991)
	Elongation ratio (ER)	$ER = 2\sqrt{(A/\pi)}/WL^*$	Watersheds with elongated shapes have a hydrological response to rainfall events with flat peaks of a long duration.	(Rogelis & Werner, 2014)
	Circularity ratio (CR)	$CR = 4\pi.A/P^{2*}$	Circular watersheds have sharper hydrographs, which means higher flashiness.	(Matauco, 2004)
	Compactness coefficient (CC)	$CC = 0.282.P^*/\sqrt{A}$	Watersheds with higher compactness coefficients are more elongated. Therefore, the hydrological response shows flat peaks of long duration.	(Islam et al., 2020)
Linear	Bifurcation ratio (BR)	$BR = SN/SN_{+1}$	It depicts the influence of structural controls in the watershed.	(Islam et al., 2020)
	Stream length ratio (SLR)	$SLR = SL/SL_{+1}$	It gives information regarding the geomorphological maturity of the watershed.	
	Stream frequency (SF)	$SF = SN^*/A$	It relates the number of streams per unit area, and therefore, the infiltration potential.	(Horton, 1945)
	Drainage density (D)	$D = SL^*/A$	It gives a general understanding of the base flow and peak flow.	(Horton, 1945)
	Constant of channel maintenance (CCM)	$CCM = 1/D$	It relates to the drainage area required to maintain one unit of channel length.	(Schumm, 1956)
	Infiltration number (IN)	$IN = SF*D$	It reflects the infiltration potential in a watershed	(Schumm, 1956)
	Length of overland flow (LO)	$LO = A/(2*SL)$	It represents the rainfall run length on the surface before reaching a defined channel.	(Choudhari et al., 2018)
Topographic	Relief (R)	$R = Z_{max} - Z_{min}$	It relates the maximum and minimum elevation inside the mapping unit.	(Mark, 1975)
	Relief ratio (RR)	$RR = R/WL^*$	It gives an idea of the sediment loss per unit area.	(Rogelis & Werner, 2014)
	Melton index (M)	M	Higher Melton indices tend to be associated with torrential watersheds.	(Wilford et al., 2004)
	Slope (S)	S_{μ}/S_{σ}	It provides an understanding of the flow velocity, erosion, and instability potential.	(Matauco, 2004)
	Profile curvature (PCR)	PCR_{μ}/PCR_{σ}	It indirectly depicts the landscape's roughness and instability.	(Schumm, 1956)
	Tangential curvature (TCR)	TCR_{μ}/TCR_{σ}	It controls the convergence of sediment material and water direction.	(Schumm, 1956)
	Topographic wetness index (TWI)	TWI_{μ}/TWI_{σ}	Accounts for topographic effect on location and size of source areas for runoff generation.	(Sevgen et al., 2019)

5.3. Suitable basic mapping unit to represent torrential flow susceptibility

5.3.1. Model validation and performance

Validating the susceptibility models allows accounting for its generalization capabilities and predictive power. Validation schemes mainly consist of susceptibility evaluation using an independent set of data. Several conceptions for generating the independent test are found in the literature. For example, Reichenbach et al. (2018) mentioned that cross-validation comprises splitting the data into training and testing sets in proportions of 70/30, respectively. Temporal partitions, where the data are split into independent time windows, are considered an optimal choice but heavily constraint for the data availability. Furthermore, k-fold cross-validation techniques can be seen as iterative processes where the data is subset into multiple independent folds used for training and validating the models at different steps (Petschko, Brenning, Bell, Goetz, & Glade, 2014). K-fold cross-validation allows using the entire data, and therefore it results in a much more detailed assessment of the model. The mentioned validation schemes are commonly implemented with the Receiver Operating Characteristics (ROC) curve and the Area Under the ROC curve (AUROC). These well-established metrics show the performance of a model at all classification thresholds.

For this research, the torrential flow susceptibility models were validated using non-spatial 10-fold cross-validation (CV). The 10-fold CV implies fitting the susceptibility model with 90% of the data and leaving the remaining 10% for testing. This procedure is repeated ten times with randomly distributed and non-overlapping folds. 10 folds can be seen as a fair value to allow the model to learn about the spatial structure from the training data (Lombardo, Opitz, Ardizzone, Guzzetti, & Huser, 2020). The ROC curve and AUROC were estimated in every iteration by comparing the fitted values with observed data to evaluate the model's predictive power.

Any susceptibility model should be spatially validated. This is since by adopting spatial CVs, one can ensure that the model estimates respect the independency assumption of the logistic regression. By spatially partitioning subsets of the study area, one then ensures that any spatial dependency is broken and does not propagate into the estimated probability values. This is particularly true for small-scale mapping units such as grid-cells, where a single grid behaves “similarly” or is statistically dependent on the adjacent ones. However, watersheds are sufficiently large mapping units to assume that the binary status and the associated covariates do not exhibit strong dependencies from the neighboring catchments. Therefore, a non-spatial cross-validation is deemed sufficient in this study.

5.4. Prioritization of areas prone to torrential flows

5.4.1. Classification of the susceptibility map

For urban planning purposes, the integration of susceptibility models can be improved by adopting user-defined classification schemes. Commonly, these schemes are developed in collaboration with decision-makers and stakeholders, which was not considered in the framework of this research. To achieve a meaningful classification, five categories were proposed based on the success rate. The success rate allows to classify a continuous spectrum of susceptibility in classes that contained a predefined percentage of the total of events.

Table 9. Susceptibility ranges based on the analysis of the success rates.

Susceptibility class	Number of events (%)
Very high	40

High	30
Moderate	15
Low	10
Very low	5

5.4.2. Integration with land-use features

The integration of land use features was done once the torrential flow susceptibility map was classified. This integration was proposed as an attempt to generate a prioritization of areas (watersheds) prone to torrential flows.

First, the watersheds with the high and very high torrential flow susceptibility classes were selected, leaving the remaining classes out of the analysis. In these two classes, 70% of the torrential flows were accumulated. Moreover, the watersheds that already evidence torrential flow events were also considered, even if classified as moderate, low, or very low susceptible areas. Secondly, from the national cartographic database, the urban centers, administrative areas such as corregimientos⁴, veredas⁵, police stations, indigenous reservations, and other EaR were extracted to assess their exposure with the susceptibility models.

Because of the mapping units, an EaR located in high or very high susceptible areas does not guarantee that the EaR is exposed to torrential flow events. For instance, this EaR can be located towards the boundaries of the watersheds, where the influence of a potentially damaging event could be absent. That is why only the EaR located within the Euclidean distance of 100 meters to the drainages were considered for further analysis.

To summarize, a watershed with historical torrential flow events or located in high or very high susceptible areas and whose EaR (urban centers and other administrative units) are within 100 meters from drainages are considered priority areas. Therefore, a more detailed analysis should be carried out.

⁴ Administrative subdivision of the rural areas of municipalities.

⁵ Administrative subdivision of the corregimientos.

6. RESULTS

The results for this section are indicated following the same order as the methods chapter. (1) watershed generation, (2) role of the predisposing and triggering factors, (3) the suitable basic mapping unit and (4) the prioritization of the watersheds.

6.1. Watershed generation

Different algorithms for watershed automatic delineation were tested to get an accurate representation of the watersheds. For example, Arc Hydro, SAGA GIS, QGIS, WhiteboxTools, HydroSHEDS (in GEE), and GRASS GIS. Initially, the algorithms were tested in relatively small areas and in a local machine (Intel® Core™ i7-5500U CPU 2.4GHz, 12GB) to check the difference between the outcomes. The delineated watersheds were visually compared against the watersheds from IDEAM (reference level, refer to section 4.6 and medium resolution watershed available in the POT of a specific municipality, Medellín).

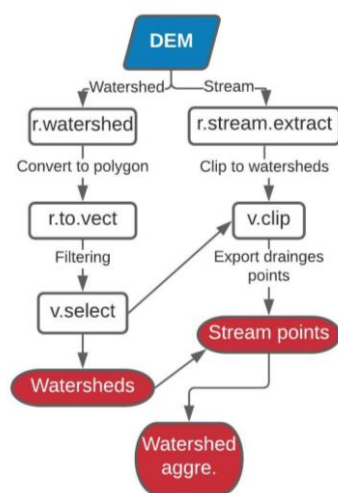


Figure 11. Scheme of the watershed generation process

Once the test for the small areas was completed, the algorithms were applied for the entire study area. For this purpose, two virtual machines owned by the Center of Expertise in Big Geodata Science at the ITC Faculty were used (Jetson AGX (8-core ARMv8.2, 32 GB GPU and PowerEdge R730xd 2 x 8-core Intel E5-2640 v3, 768 GB). However, the processing time played an essential role since several of the tested algorithms were not able to process the entire study area at once, and in fact, failed after some time of processing.

GRASS GIS was chosen to delineate the watersheds since it provided consistent watersheds polygons and allowed the aggregation of the drainage network in the watershed (stream length, number of streams, Strahler order).

A brief overview of the step sequence implemented in GRASS GIS for the watershed and drainage network generation is provided in Figure 11.

The watersheds and the stream network were generated from the DEM using the same flow accumulation thresholds. After that, the watersheds were filtered using the region of interest, and the streams were clipped to the selected watersheds. The streams were exported as point geometries, in which later the accumulation flow was extracted per point. The lowest accumulation flow value in every watershed was extracted as the outlet point associated with a watershed polygon. Using the point outlets, the watershed polygon, and the DEM, the Watershed Length (WL) was estimated as the distance between the outlet point and the point with the highest elevation within every watershed. Recall in Table 8 that the WL was used to calculate several of the morphometric indices. Furthermore, information regarding the number of streams, stream length, and Strahler order were extracted into the watersheds to calculate the remaining morphometric indices.

This procedure was carried out to delineate the different watershed levels and aggregated their stream network characteristics. The results of the watershed generation are summarized in Table 10 and shown in Figure 12. Moreover, the scripts used to generate the watersheds can be found in Appendix 10.5.

Table 10. Compilation of the generated watersheds. The number in the first columns corresponds to the minimum size of the exterior watershed basin.

Level	Number of watersheds	Average area
0 - IDEAM	223	2,750 km ²
1 - 50,000	713	750 km ²
2 - 25,000	1,445	360 km ²
3 - 10,000	3,598	145 km ²
4 - 5,000	6,906	75 km ²
5 - 1,000	32,293	15 km ²

Note that the number of watersheds is only summarized for the region of interest, not the entire country.

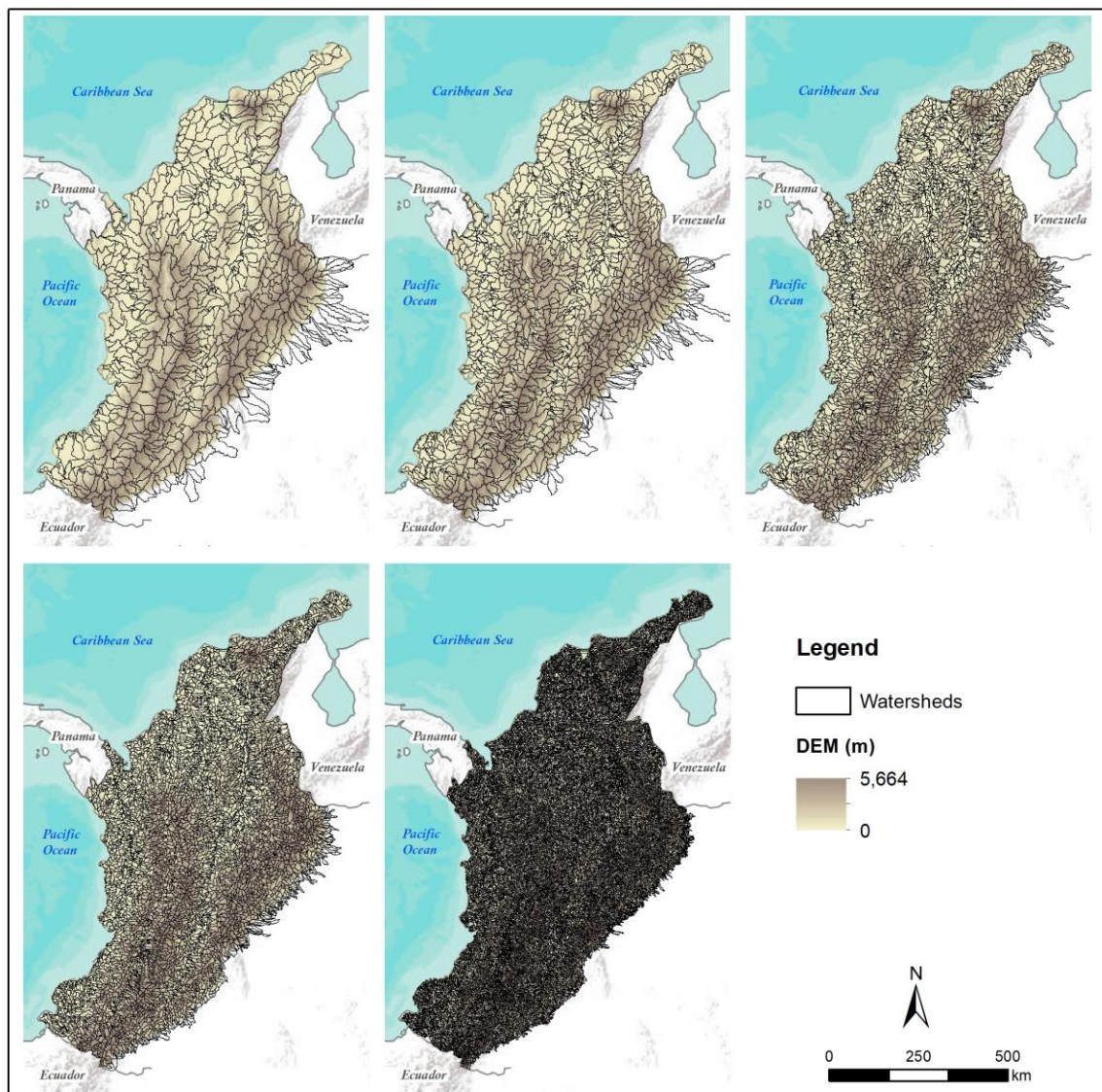


Figure 12. Overview of the different levels of delineated watersheds. From left to right and from top to bottom, watershed level 50,000, 25,000, 10,000, 5,000 and 1,000.

6.2. Role of the predisposing and triggering factors in the occurrence of torrential flow events

6.2.1. Multi-collinearity

Figure 13 shows the results of the multi-collinearity test for the morphometric indices. The test was initially computed for all the pairs of covariates. However, since there were not strong relationships between covariates from different groups, and for illustration purposes, the Pearson matrix was divided into the groups of predisposing factors (morphometric indices, geology, land cover-land use, and rainfall). The remaining matrices can be found in appendix 10.5.

The circularity ratio (CR) and the compactness coefficient (CC) show a solid negative relationship in the areal indices. Therefore, CC was discarded considering the information that the two indices can add to the susceptibility model. For the linear indices, stream frequency (SF) showed a moderately high relationship with the drainage density (DD) and the infiltration number (IN), which are the reasons why SF was not considered for further analysis. Following the same idea, constant of channel maintenance (CCM) and infiltration number (IN) were left out due to their strong relations with drainage density (DD) and length of overland flow (LO), respectively. In the group of the topographic factors, the vast majority presented collinearity issues. This behavior is most likely explained by the dependence of the morphometric indices on the slope angle (elevation differences or relief). The mean basin slope ($S\mu$), the mean tangential curvature, and the mean topographic wetness index were preserved from this group. The remaining indices were discarded.

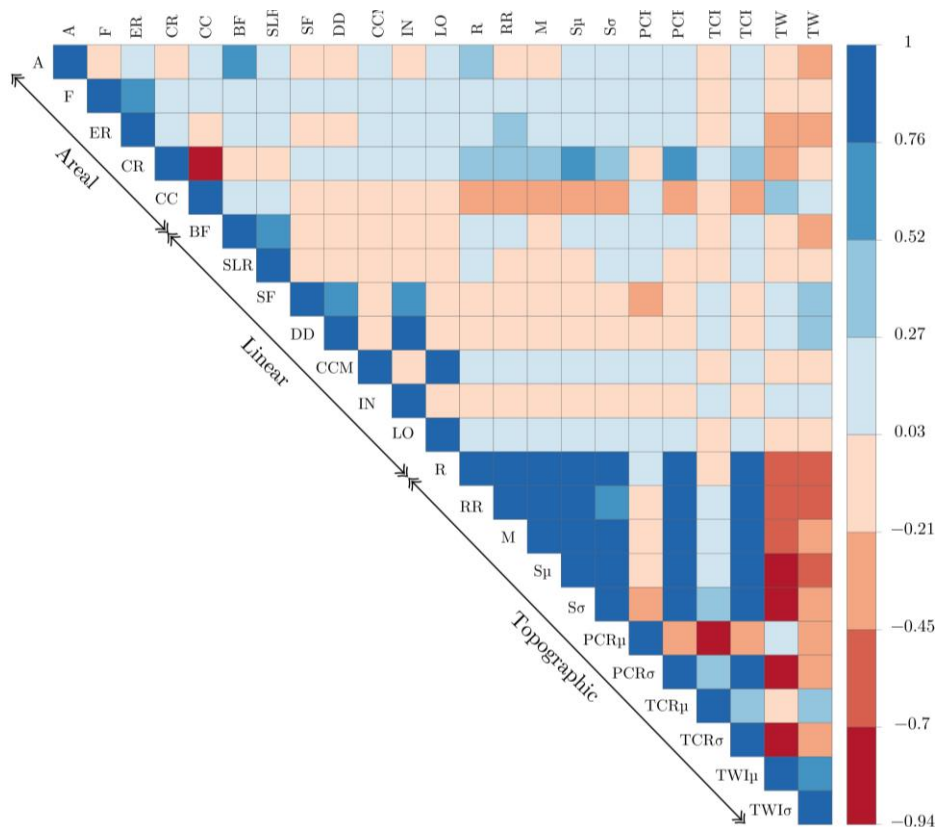


Figure 13. Multi-collinearity test for morphometric indices. Abbreviations according to Table 8. >0.75 or >-0.75 were taken as thresholds to indicate whether the pair of covariates show strong relations or not.

Serpentinite, phyllite, schist, and marble were excluded from the geology since they present strong relationships with quartzite. These five lithological types appear to be strongly associated since they are often found in the same lithological units, especially in the Andean mid-range. Refer to the Appendix 10.8

Although significant correlations were expected in the proportions of land cover and land use, the Pearson matrix showed that only the pairs of artificial land/residential areas and inland water/water bodies presented strong correlations. Besides, classes such as clouds, coastal and inland wetlands, and marine waters were not further considered since, from an interpretative viewpoint, they are not relevant for explaining torrential flows. Refer to the Appendix 10.10.

Finally, the total annual rainfall (μ) and total annual rainfall (σ) show strong correlations with the average daily rainfall (μ) and average daily rainfall (σ) respectively. Therefore, to represent general rainfall conditions, the average daily rainfall (μ , σ) was selected over the total annual values. Recall (μ) refers to the average per watershed and (σ) represents the standard deviation per watershed 10.9

6.2.2. Covariate effects

Linear effects

Figure 14 depicts the posterior distribution of the covariates estimated to be significant for Mod1 (SIMMA inventory) and Mod2 (DesInventar inventory). Recall that SIMMA represents source areas and DesInventar impacted areas. In general terms, Mod1 is explained by the covariates related to land cover and land use, while the morphometric indices and land use explain Mod2. Recall that Mod1 is representing watersheds where torrential flows are generated, and Mod2 watersheds impacted by them.

For Mod1, it is observed that positive values are shown for morphometric indices and the land cover classes. In contrast, the negative contributions are observed for the lithological and land-use factors. Covariates such as area, $PRC\mu$, the proportions of conglomerates, tuff, artificial land, forest plantation, and badlands appear to have the narrowest credible intervals even if their RCs are not necessarily the highest ones (in absolute values). Conversely, the remaining covariates show strong positive and negative influences, but the CIs are relatively wider than the mentioned covariates, making it difficult to build solid interpretations other than their positive/negative contributions.

Remarkably, while land cover classes such as arable land and permanent crops positively explain the source areas for torrential flows, the agriculture (potential) land use reflects the opposite. Recall that the land use map refers to the potential land use that a land mapping unit could have, which in principle does not imply a match with the land cover maps. Besides, the two products were produced by different institutions in Colombia in different time periods. This behaviour is also found between forest plantation and forest production.

In Mod2, covariates with relatively narrow CIs are Area, Circularity Ratio, Bifurcation Ratio, $PCR\mu$, $TWI\sigma$, and the proportion of surface deposits, conglomerate, artificial land, arable land, and forest plantation. At the same time, most of the covariates present a positive contribution to the susceptibility model except for drainage density, circularity ratio, and the proportion of andesite.

Unexpectedly, the Circularity Ratio (CR) and Drainage Density (DD) depicted a negative influence, which means that elongated watersheds (low CR) with permeable materials (low DD) can increase the chance of a watershed being impacted by a torrential flow. Also, the Bifurcation Ratio and the proportion of

deposits positively influenced the model, meaning highly dissected watersheds with significant deposits have higher chances of being impacted by a torrential flow.

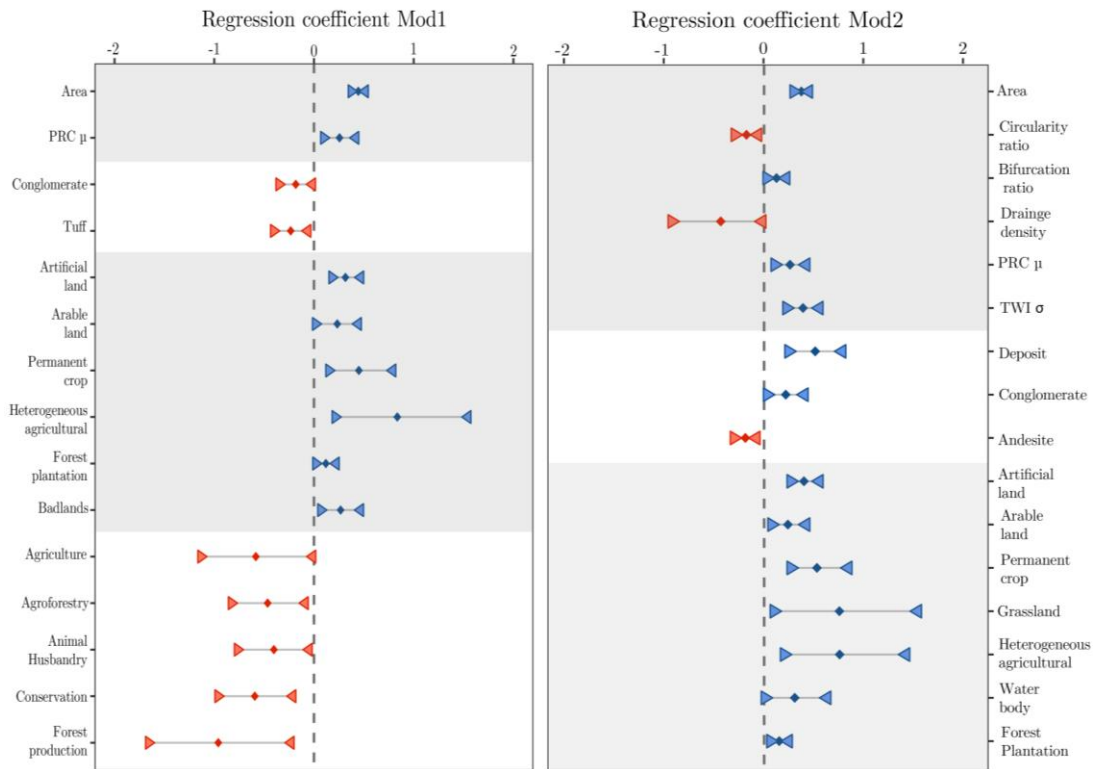


Figure 14. Linear effects (significant) for Mod1 and Mod2. The y-axis reports the covariates with the respective regression coefficients in the x-axis. Diamonds depict the mean of the posterior distribution for each RC. Triangles show the 95 credible intervals of the RC posterior distribution. In red, the negative mean RCs, in blue, the positive ones. The grey boxes divide the covariates into the previously established groups (morphometric indices, lithology, land cover-land use, and rainfall).

Non-linear effects

Initially, all the covariates were modeled as linear effects, but based on the significance plots and the geomorphological importance, four covariates were modeled using a random walk structure defined over 20 quantile classes to capture potential nonlinearities. Figure 15 reports the random effects of ordinal non-linear covariates for Mod1. Since the plots for non-linear effects in Mod2 were almost the same as Mod1, they are not shown here.

For the form factor, the mean contribution to the model is positive, except for the values below ~ 0.5 , although the effect is primarily non-significant. The Slope(μ), as expected, has the most substantial contribution to the model with very a narrow CI in its entire distribution. It is positive for values higher than approximately 10° , and overall, it shows linearity.

Average daily rainfall μ has, in general, a mean negative influence on the model excluding rainfall values lower than ~ 7 mm. After ~ 7 mm, the CI becomes even more uncertain due to the lack of observations for that range. Overall, it does not seem to be significant. Lastly, the maximum daily rainfall showed negative contributions for rainfall measures lower than 130 mm. After that, it depicted positive influences that become significantly step after values of 200 mm

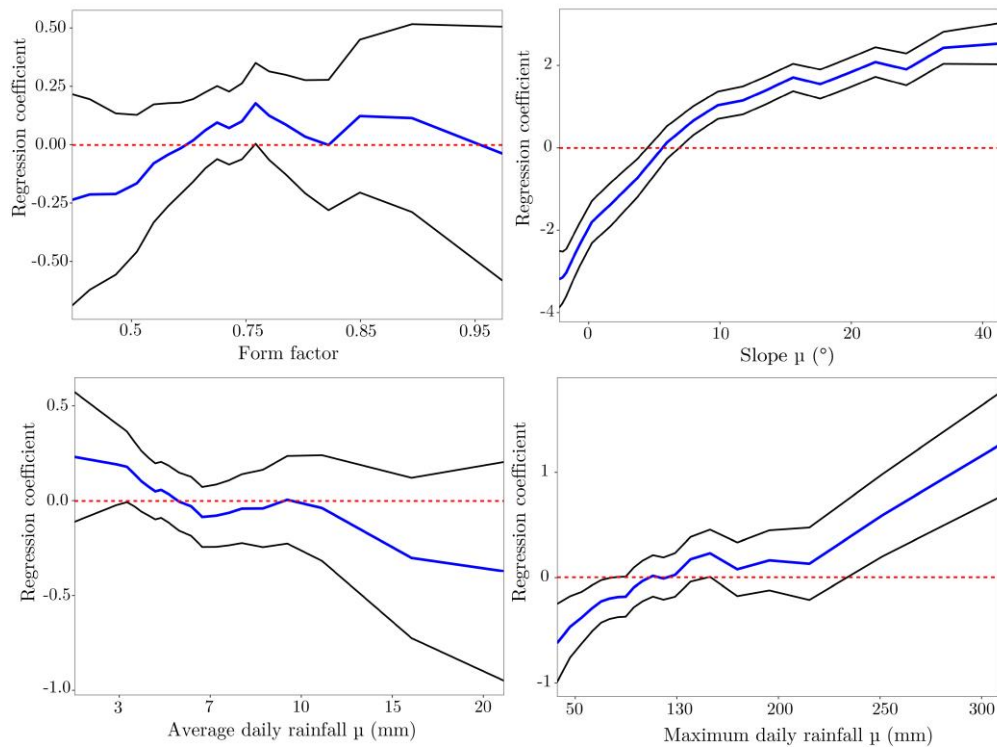


Figure 15. Non-linear effects in the susceptibility models. The blue line summarizes the mean of the posterior distribution for the RC, and the black lines are the 95% credible interval.

6.3. Suitable basic mapping unit to represent torrential flow susceptibility

6.3.1. Model validation and performance

After concluding the exploratory model based on the significance of the linear and non-linear effects, the 10-fold cross-validation and ROC curves were implemented to evaluate the susceptibility models' performance quantitatively.

Figure 16 shows the ROC curves obtained for the 10-fold cross-validation of Mod1 and Mod2. The results for all the watershed levels and the two models are summarized in Table 11.

The median values of the AUROCs for all the models are considered as excellent discriminations according to Hosmer and Lemeshow (2013). Overall, it is clear that the AUROCs tend to decrease as the resolution of the watershed increases, although not to large extents. Also, Mod1 shows in all the watershed levels slightly better performances as compared to Mod2. Recall that Mod1 was built upon the SIMMA inventory, which is mapped with fieldwork support, whereas Mod2 is built upon the DesInventar database, in which the author manually georeferenced the events. Therefore, the results could be strongly influenced by the spatial errors in the location of events.

The applicability of a susceptibility model relies to some extent on how certain the estimated mean susceptibilities are (see Figure 17). The CI, in principle, should be narrow and exhibit minor uncertainties towards the extreme values, i.e., stable and unstable areas, and follow a bell shape (Lombardo & Tanyas, 2020). However, this appears to be the case neither for Mod1 nor Mod2. The mean susceptibilities do not show relatively high values, and they seem to be almost constrained to probabilities below 0.5. This could be strongly influenced by the imbalanced nature of the dataset, especially for level 1,000. In other words,

the dataset contains a lot more stable than unstable watersheds, which results in right-skewed posterior mean susceptibility distribution.

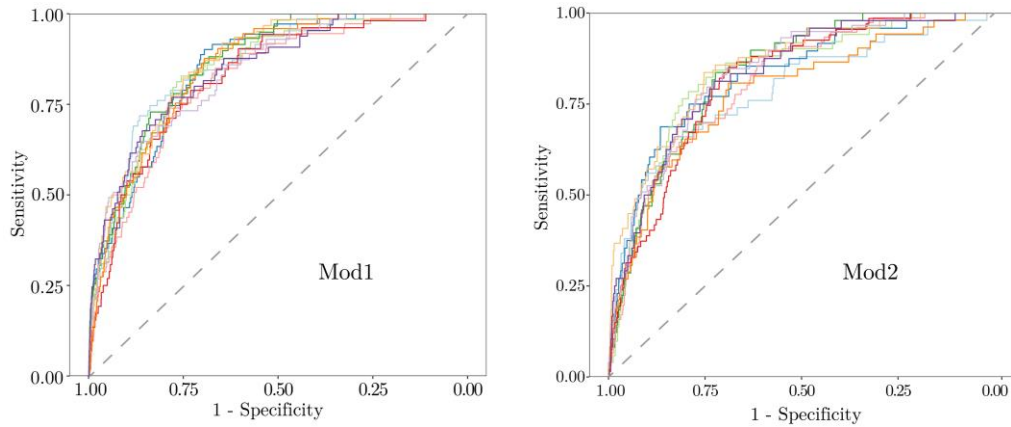


Figure 16. Illustration of the ROC curves (Mod1). Every solid line represents the ROC curve associated with each one of the ten folds. The dashed line shows a theoretical random model (with AUROC = 0.5).

Table 11. Report of the performance results. Median AUROC values are shown for Mod1 and Mod2 for all levels of watersheds.

Level	Mod1	Mod2
50,000	0.87	0.86
25,000	0.86	0.83
10,000	0.86	0.82
5,000	0.85	0.82
1,000	0.85	0.82

Remarkably, Mod2 reports very high uncertainties for low mean susceptibilities. Indeed, this is not an optimal situation since, for low mean susceptibilities, the model ideally should depict low uncertainties. Once again, this behavior could be a reflection of the positional errors and incompleteness in the DesInventar inventory. Therefore, a new modeling option was introduced to deal with that. The new model is further referred to as Mod3.

Mod3 is built under the assumption that torrential flows can be generated (source areas) and impact the same mapping unit, i.e., the same watershed. In that sense, the inventories corresponding to the source points (SIMMA) and impacted areas (DesInventar) were combined into a single inventory. In principle, there should be an overlapping between the two inventories; every event should have a source and an impacted area. Nevertheless, due to the spatial and temporal uncertainties in the information, checking whether two points represent the same torrential flow event was not possible.

Based on the results presented in Figure 17 for Mod2, the watersheds with low susceptibility but high uncertainty values were manually removed from the combined inventory. This approach was taken to account for those potential errors in the spatial location of the DesInventar inventory.

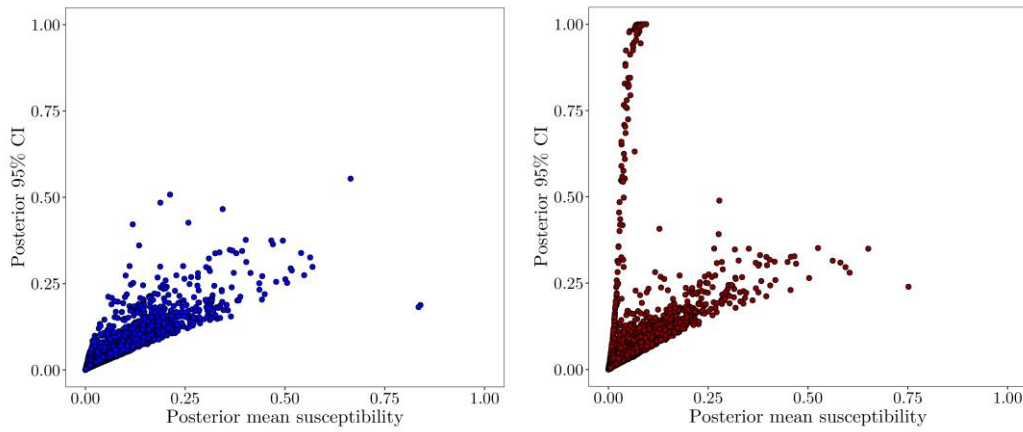


Figure 17. Posterior 95% CI vs. posterior mean susceptibility for the watersheds at level 1,000. Blue corresponds to Mod1 and red to Mod2.

All the previous analyses were repeated using the new combined inventory (SIMMA + corrected DesInventar inventories). Table 12 depicts the performance results, and Figure 18 the error plot related to the posterior mean susceptibility and the 95% CI. Compared to Mod1 and Mod2, there were no significant differences in terms of performance. On the other hand, the error plot has a more defined bell-shaped distribution, with very few watersheds showing high uncertainties in the distribution's tails. Illustrations of the spatial realizations and uncertainties for the torrential flow susceptibility at each watershed level are shown in Figure 20, Figure 21, and Figure 22. Furthermore, the complete error plot for the three models and all the watershed levels can be found in appendix 10.11.

Table 12. Report of the performance results. Median AUROC values are shown for Mod3 for all levels of watersheds.

Level	Mod3
50,000	0.87
25,000	0.86
10,000	0.85
5,000	0.84
1,000	0.84

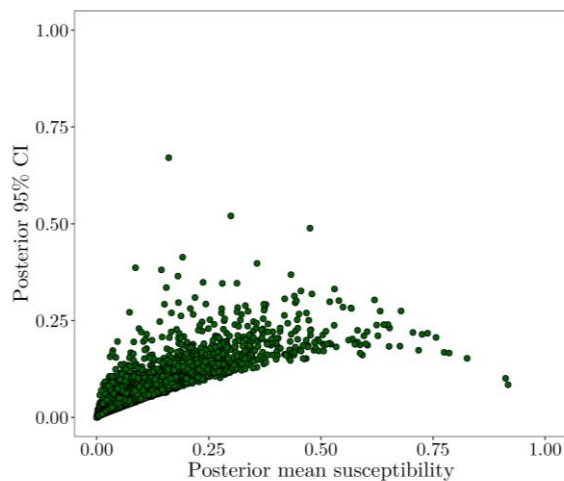


Figure 18. Posterior 95% CI vs. posterior mean susceptibility for Mod3.

Results indicate that performance-wise, the coarser resolutions show higher performances, and overall, for the three models, the coarser the watershed levels, the higher the performances. However, in terms of the error plots, the more detailed watershed levels show lower uncertainties.

Although the five models have a wide variety of resolutions, they all can generate, quantitatively speaking, good predictions for the torrential flow susceptible watersheds. Besides, since this study focuses on prioritizing areas based on their torrential flow susceptibility, the more detailed levels of watersheds such as 5,000 and 1,000 may represent

better options for this goal. Finer watersheds can provide more spatial details, which appears to be more meaningful for urban planning applications at municipal levels. Consequently, the prioritization assessment was carried out only for the two most detailed levels of watersheds (5,000 and 1,000).

6.4. Prioritization of areas prone to torrential flows

6.4.1. Classification of the susceptibility map

The results of the susceptibility map were then classified using the success rate. Due to the lack of information regarding the area of the events, the success rates for every watershed level were computed using the number of torrential flows events. Figure 19 illustrates an example of the calculated success rate for level 10,000 in Mod3.

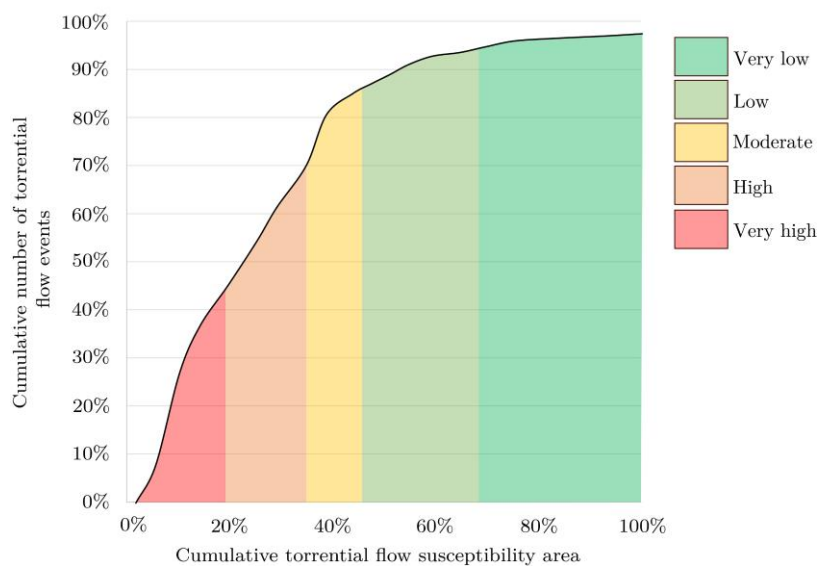


Figure 19. Success rate for Mod3. The color palette represents the previously established classes in Table 9.

Table 13 depicts the distribution of percentages for every susceptible class and every watershed level. The percentages of susceptible classes show consistency among the different evaluated levels. Larger watersheds have higher percentages of very high and high susceptible areas compared to the finer watersheds. In contrast, finer watershed levels present higher low and low susceptible proportions than larger watersheds. Overall, the proportions for different levels seem to follow a trend except the level 5,000, where the reported percentages slightly deviate from the rest.

Table 13. Percentage of susceptibility classes for each watershed level (Mod3).

Level	Proportion of susceptibility classes (%)				
	Very low	Low	Medium	High	Very high
50,000	35	16	18	14	17
25,000	35	17	18	15	14
10,000	34	16	20	16	13
5,000	47	20	16	7	11
1,000	42	16	23	11	9

Below, the torrential flow susceptibility and uncertainty for all the watershed levels. Note that the uncertainty was classified using the quantiles of each distribution. Even if the same color style was used, every watershed level has independent uncertainty classes

The torrential flow susceptible maps show consistency among the different watershed levels. A visual inspection gives the idea that the susceptibility follows a potential hierarchical structure among watersheds. For example, the watersheds with high or very high susceptibility in level 50,000 match groups of watersheds with high or very high susceptibility in level 25,000. Also, similar behavior is seen for the remaining levels, although with some exceptions, especially evidenced in flat areas.

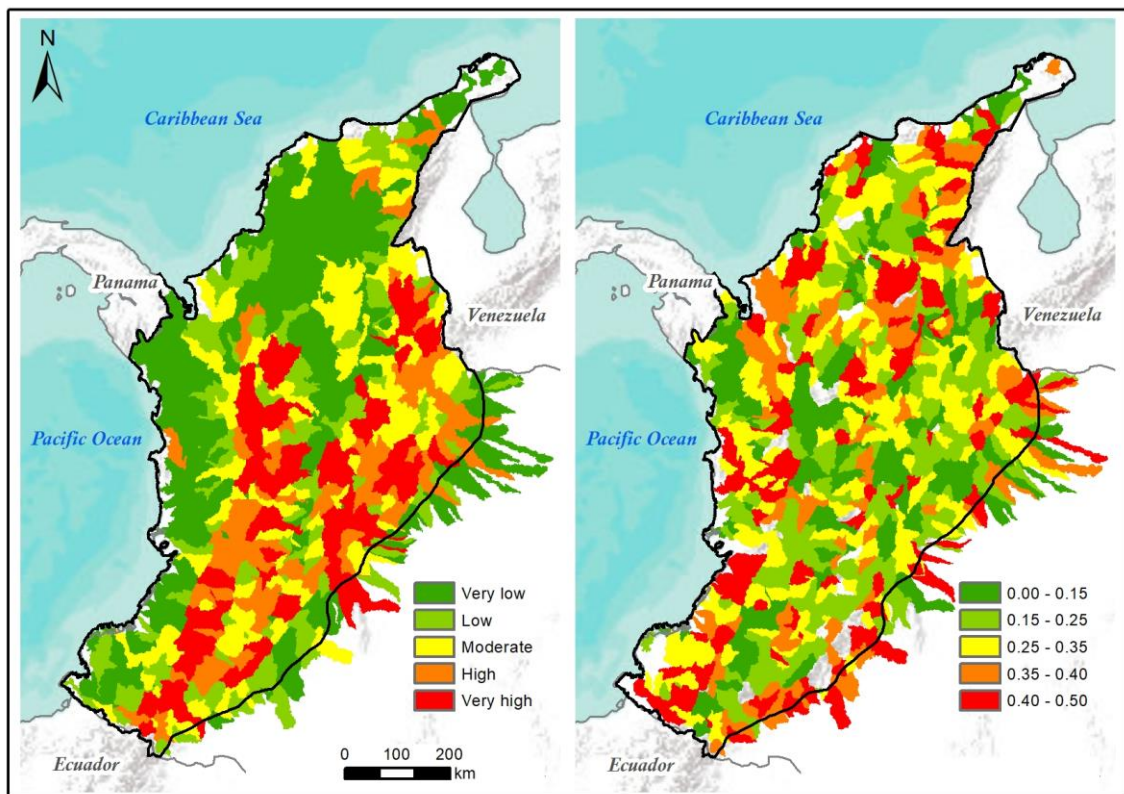


Figure 20. Results for the watersheds in Level 1-50,000. The map on the left side shows the torrential flow susceptibility classes for Mod3, whereas the map on the right indicates the corresponding 95% credible interval.

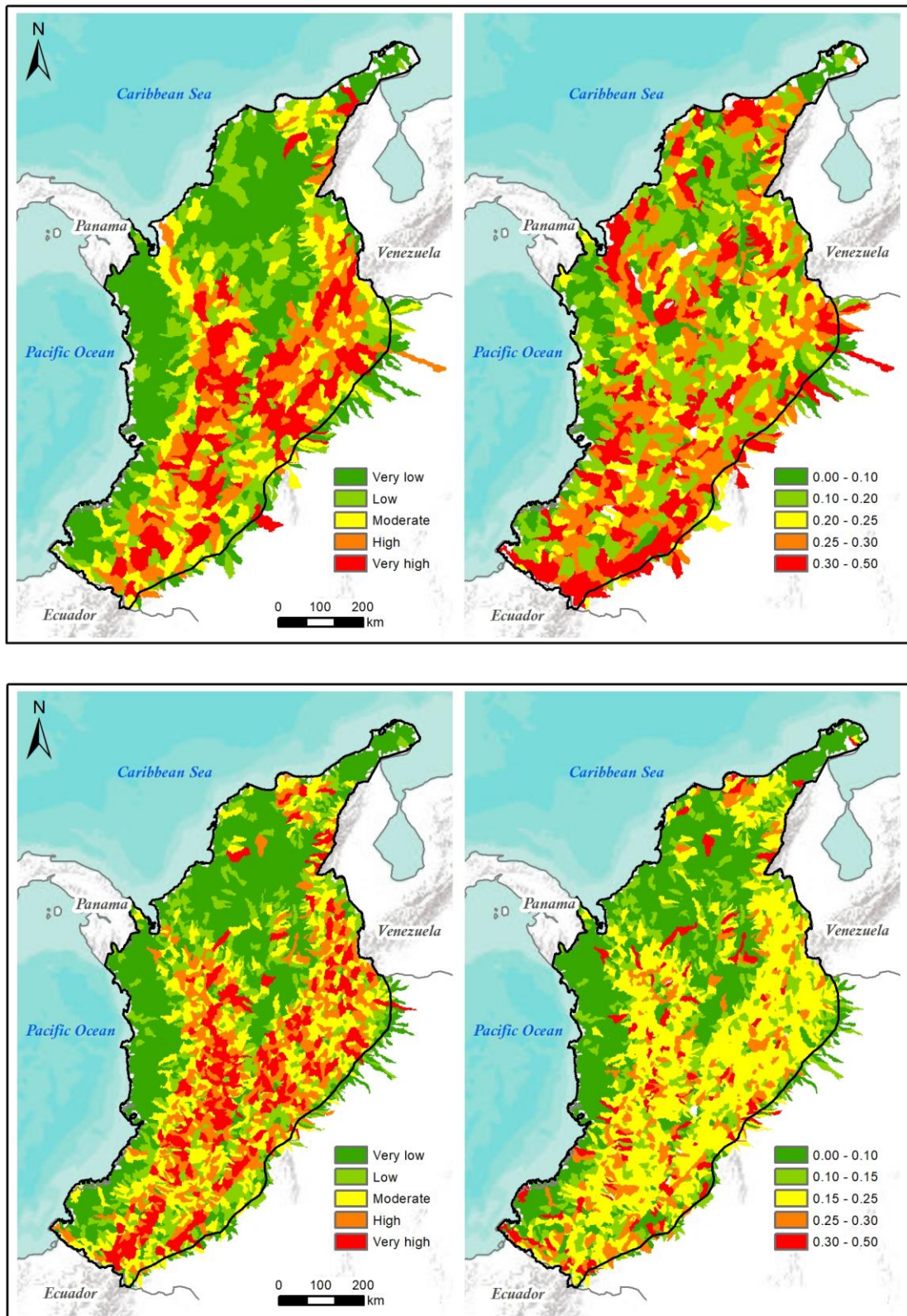


Figure 21. Results for the watersheds in Level 2-25,000 (top) and Level 3-10,000 (bottom). The map on the left side shows the torrential flow susceptibility classes for Mod3, whereas the map on the right indicates the corresponding 95% credible interval.

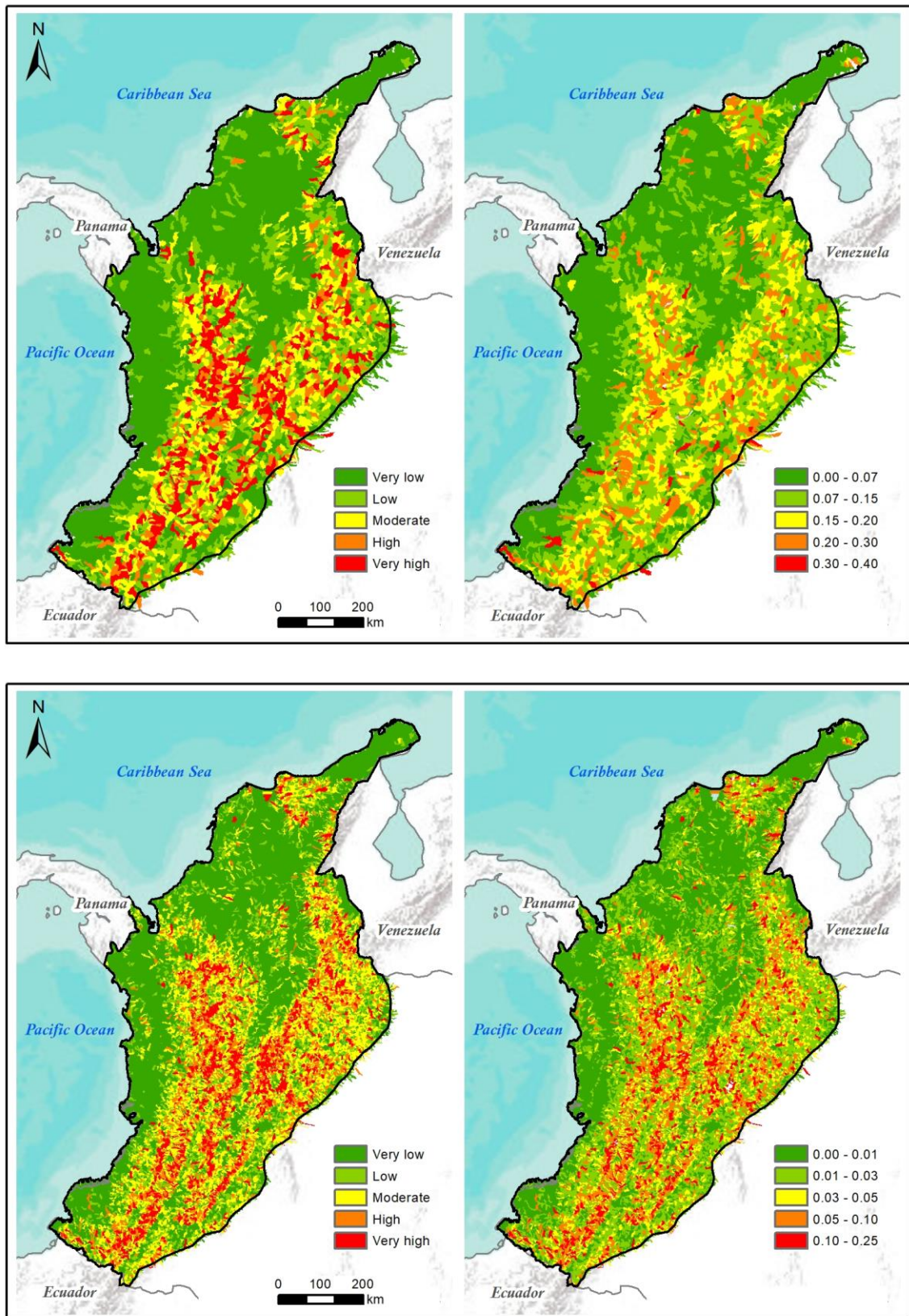


Figure 22. Results for the watersheds in Level 4-5,000 (top) and Level 5-1,000 (bottom). The map on the left side shows the torrential flow susceptibility classes for Mod3, whereas the map on the right indicates the corresponding 95% credible interval.

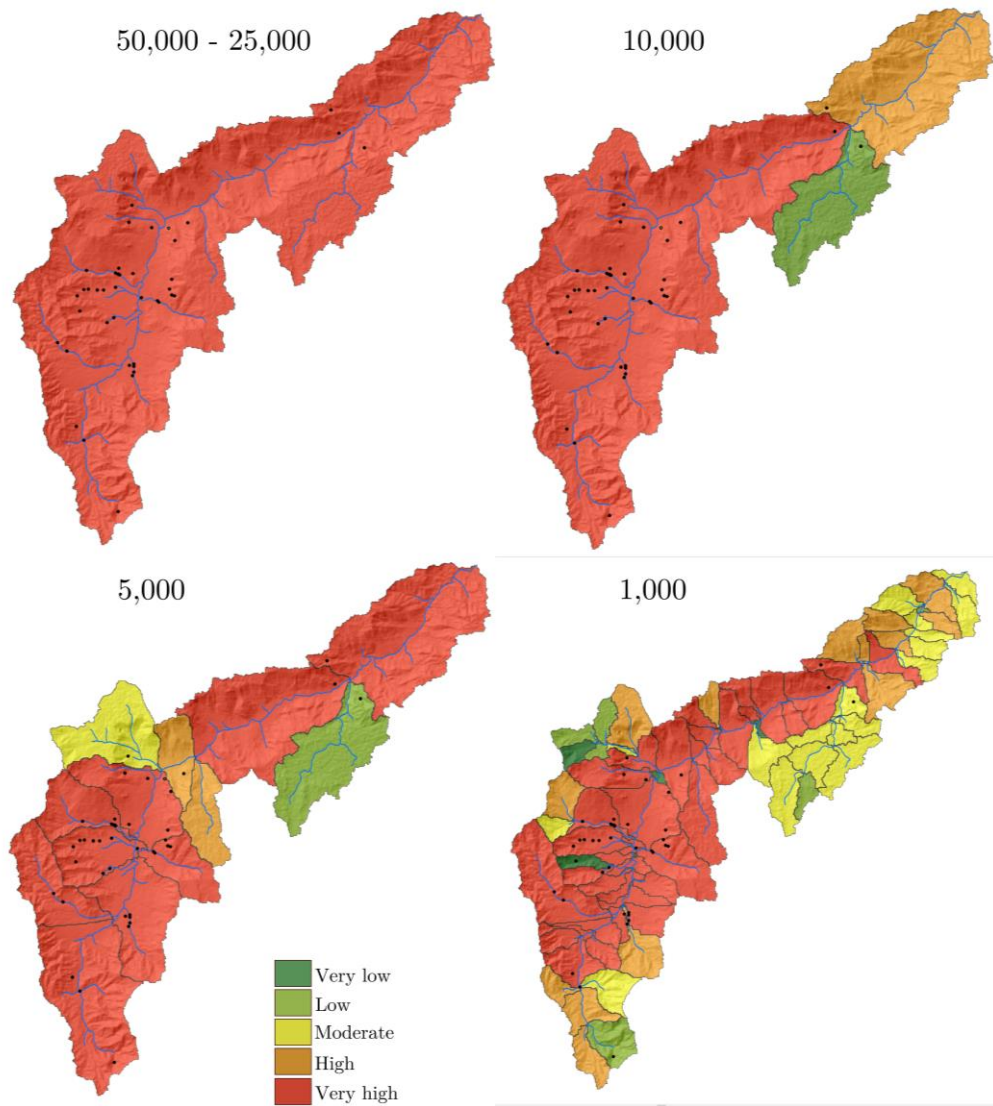


Figure 23. Comparative overview of the different watershed levels. Note that since the levels 50,000 and 25,000 were equal (particularly for this area), they refer to the same panel.

Figure 23 shows the susceptibility in the different levels of watersheds (hierarchical structure). As seen, very high susceptible watersheds in the coarse levels seem to be classified as high or very high susceptibility areas by the remaining levels.

6.4.2. Integration with land-use features

The incorporation of EaR is done once the susceptibility maps are generated and classified. The prioritization was done by selecting watersheds with (1) high or very high susceptibility class, (2) historical events (3) presence of urban centers or small settlements.

Figure 24 shows the results of the prioritization procedure using the previously described EaR, and the high and very high susceptible watersheds. As shown, most of the prioritized watersheds are clustered in the central part of the country with, some cases, although very few, towards the north and western coasts.

Results show 871 and 429 prioritized watersheds with an estimated area of 21,600 km² and 51,900 km² for the levels 1,000 and 5,000, respectively. At the same time, these prioritized watersheds are located in 671 and 709 municipalities, representing 60% and 63% of the total number of municipalities in Colombia, respectively.

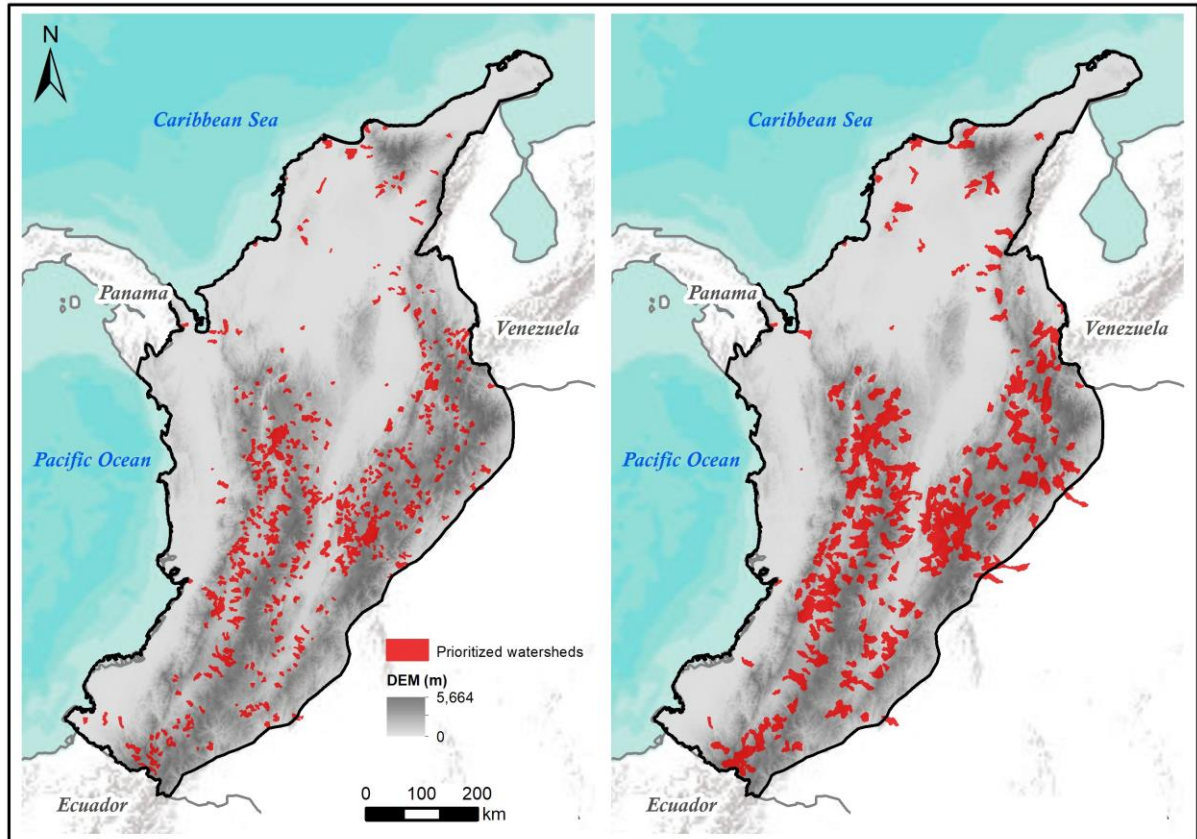


Figure 24. Prioritized watersheds for levels 1,000 (left side) and 5,000 (right side) for Mod3.

7. DISCUSSION

The discussion will address the issues in the same order as presented in the results chapter.

7.1. Covariate effects

The morphometric indices did not seem to play a relevant role as explanatory covariates. As a matter of fact, only 5 out of 25 indices were significant for at least one of the models. Among those five significant indices, Drainage Density (DD) and Circularity Ratio (CR) appeared to influence the susceptibility negatively. Hence, torrential watersheds in Colombia would have low drainage densities as well as low circularity ratios, which following the interpretation of the indices, could be translated into watersheds with permeable materials and elongated shapes. In principle, it is contradictory since watersheds with permeable materials imply slow hydrological responses and less runoff generation. Also, elongated watersheds have hydrographs with flat peaks of long duration in response to rainfall events. These results are consistent with the previous research done in Colombia by Arango et al. (2020), suggesting that torrential watersheds in Colombia are effectively elongated and contain relatively permeable materials.

Conversely, the Bifurcation Ratio (BF) shows a positive effect, meaning that highly dissected watersheds in mountainous areas tend to be more prone to torrential flows. Nevertheless, these geomorphic inferences should be avoided as long as the models were produced with highly incomplete data (Steger et al., 2016). Moreover, the strange role of the DD and BF could be potentially showing collinearity issues that were not detected during the analysis, and therefore, it would be valuable to consider other methods to assess the selection of the variables.

An important aspect is also the incompleteness of the historical inventories. In this research, a relatively large area in Colombia could be modeled with highly incomplete inventories. When referring to the performance, the obtained results were considered as excellent discriminations (Hosmer et al., 2013). However, this was not the case for the interpretation and understanding of the role of the covariates. Concluding or linking between covariates and torrential flows could not be done appropriately within this research. A potential reason for those strange relations found might be the incompleteness of the inventories. For instance, looking at Figure 3, especially for the SIMMA inventory, it is easy to identify areas where mapping campaigns have been conducted. Those areas are relatively more complete since, in the same mapping unit, they have more events. When this is the case, High data incompleteness can wrongly lead to having over or underrepresentation of the data. Therefore, before analyzing geomorphic influences with highly incomplete inventories, other sets of approaches should be considered, i.e., the mixed effected models (S. Steger, Brenning, Bell, & Glade, 2017).

According to the results, the lithology did not show important contributions to the susceptibility estimation. A potential reason could be the disaggregation procedure during the data preparation. Although the conducted process provides a general parametrization of the lithological compositions, it does not reflect the local conditions of the geological units, which could add relevant information for the analysis. Another drawback is that the described procedure treats every lithological class as an “independent class”, while perhaps the torrential flows could be better explained by the combination of lithologies in the same geological unit. In that sense, a combination of a detailed exploration of the lithological classes and the incorporation of in-depth local expertise to determine specific geological units of interest could provide more helpful information to the model and potentially improve the analysis. Also, another perspective will be the determination of physiographical regions of analysis (Wang et al., 2021). These regions could be built upon geological and geomorphological information that would potentially allow accounting for the differences in the local geological conditions

Another critical point to be addressed is the aggregation of the covariates into the mapping units. Whereas continuous covariates were aggregated using mean and standard deviation, categorical covariates were aggregated through the proportions (percentage cover) of each class in every mapping unit. This type of aggregation technique has shown successful results when it is done in slope units (Lombardo et al., 2020). For the case of watersheds, geomorphologically speaking, they include larger areas and a much more heterogeneous landscape diversity, making the use of mean and standard deviation perhaps not the best representation. This was evidenced, especially in the coarser levels, where homogenous values with a limited number of observations were produced by the aggregation process and increased the model's global uncertainties.

During this research, only rainfall was included as a triggering factor. However, the author considers it strongly important to explore the role of other initiation mechanisms such as earthquakes, volcanoes, glacial and anthropogenic ones related to mining activities and dam breaks. For instance, in 1994, about 3,000 landslides, triggered by a 6.4-magnitude earthquake, reached the Páez river generating a debris flow event that caused severe losses. Also, another well-known case is the Amero tragedy in 1985, in which a torrential flow (lahar) was triggered by the eruption of the Nevado del Ruiz volcano.

The temporal effects of the rainfall as a triggering factor could be potentially improved if different rainfall variables were integrated based on the dates in which the torrential flows occurred instead of using only a single rainfall representation. However, this analysis would have three main difficulties: (i) some of the events occurred on dates where the rainfall information was not yet available (before 1980), which might lead to potentially lose part of the information. (ii) when analyzing rainfall measures, especially for intense events (which are likely associated with the occurrence of torrential flows), minor inaccuracies in the date of the torrential flow might lead to a wrong interpretation of the results; therefore, a more robust preparation and temporal uncertainty of the inventories is crucial. (iii) aggregating the rainfall information into the mapping units, watersheds, in this case, would represent a challenge since the stable watersheds (where there are no torrential flow events) could not have the same representative rainfall value. An average or maximum rainfall value could be used for the specific case of those (stable) watersheds.

7.2. Suitable mapping unit to model to represent torrential flow susceptibility

In this research, several sources of information with different spatial resolutions and time periods were integrated to estimate torrential flow susceptibility. In this procedure, it is essential to highlight all the potential uncertainty sources involved. For example, Guzzetti et al. (2006) mentioned four primary sources of uncertainty: the errors in the inventory and thematic information available, lack of understanding of the phenomenon of interest, limitations in the techniques used to estimate susceptibility, and the natural variability of the phenomena. In this particular case, substantial uncertainties regarding the inventories and thematic information are identified.

Performance-wise the susceptibility results did not depict significant differences among the five watershed levels. Even, after its reclassification was done according to the success rates, the different watershed levels showed consistency under visual inspection. However, remarkable differences were found in terms of uncertainties. The larger the watersheds, the higher the associated uncertainties, which was an important consideration when selecting the suitable mapping units for the prioritization step. Also, choosing the best watershed level should consider the goal of the potential application of the maps. For this research, the watershed levels with the lowest relative performances were selected because of their low uncertainty values and the more meaningful information they could provide for prioritizing areas.

A watershed, as a landscape unit, comprises a variety of geomorphological processes. The top parts are dominated by erosion processes, the middle by transport processes, and the lowest by deposition processes (see Figure 25). In that sense, it is expected that the torrential flows are originated in the erosion zones, flow through the transport zones and finally reach the deposition zones. Hence, subdividing a watershed according to its dominant process (at least erosion and deposition) would better represent the torrential flow modeling. At a national scale, this analysis would be challenging. A not-so-complex approach would be establishing thresholds; for example, based on topographical factors such as slope, relief, and their numerical distribution for each watershed (by quantiles or natural breaks), define at least two classes. One class would correspond with the Zone 1 and the other one with Zone 2 + Zone 3. Rerunning the entire analysis with these new mapping units would potentially provide better results.

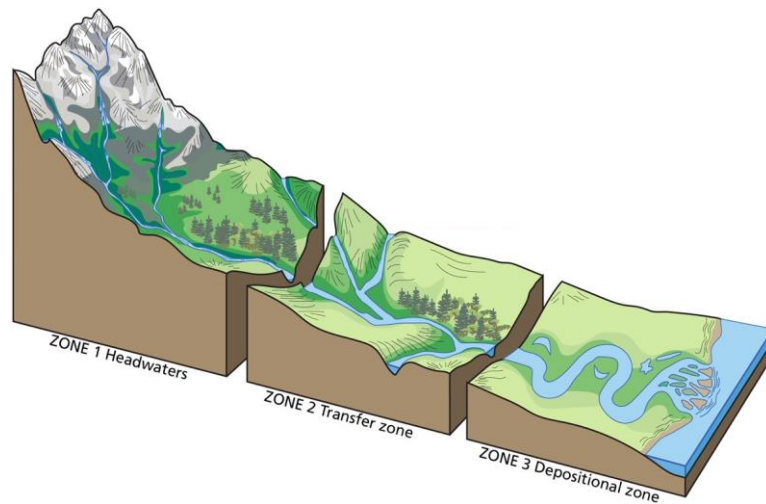


Figure 25. Watershed subdivisions. Modified from <https://www.nps.gov/subjects/geology/fluvial-landforms.htm>

8. CONCLUSIONS

In the current climate change scenario, frequencies and intensities of extreme events are expected to increase in the upcoming years, likely leading to an increase in torrential flow events. When there are exposed EaR, the society tries to respond by implementing different risk reduction measures, for which hazard or at least susceptibility models should be analyzed as important components within the urban planning regulations.

During this research, an innovative data-driven approach, GAM in a Bayesian framework, was exploited to provide a first attempt at a torrential flow susceptibility model at a national scale in Colombia. Afterward, the susceptibility was analyzed in combination with several EaRs to prioritize areas prone to torrential flows.

The susceptibility modeling involved a vast data processing component on the integration and parametrization of multiple data sources. For example, two torrential flow inventories were considered to carry out the assessment. 1363 torrential flow events of the DesInventar inventory were manually georeferenced based on each event's description. Furthermore, several levels of watersheds were considered and compared during the analysis to find a suitable landscape partition to represent the torrential flows. In terms of the variables, morphometric indices, lithology, land cover-land use, and rainfall were retrieved, pre-processed, parametrized, and aggregated into the considered watershed levels as part of the dataset construction.

As part of the modeling settings, a multi-collinearity assessment was conducted to leave out of the analysis potential variables in conflict. Mainly, substantial collinearity issues were detected among the morphometric indices. Then, initial exploratory models for each of the inventories were conducted to understand the influence and significance of the predisposing and triggering factors related to torrential flow susceptibility. Results highlighted variables such as slope and maximum daily rainfall for having the strongest influences in the model. Due to the inconsistency, it was questionable whether the role of some morphometric indices such as Circularity Ratio, Drainage Density, and Bifurcation Ratio could explain logical relations regarding the torrential flow events. Besides, the lithological variables did not show the expected tendencies, so it is recommended to incorporate other parametrization and aggregation techniques.

K-fold cross-validation and AUROC metrics were implemented to address the validation and performance of the susceptibility model in the different levels of watersheds. Results were consistent and did not depict substantial differences in terms of the performances; however, they did indicate differences when analyzing the uncertainties. Therefore, the selected suitable watersheds were based not only on performance metrics but also on uncertainty and noticeably the study's goal, which was prioritizing areas for spatial planning purposes.

Due to the scale of the analysis, the prioritization of watersheds was done considering elements at risk, such as urban centers and smaller settlements within a 100-m distance from the main streams. The results showed that 871 and 429 watersheds for the levels 1,000 and 5,000 respectively should be prioritized. Therefore, detailed studies should be conducted on those areas.

9. ETHICAL CONSIDERATIONS

As stated during the previous sections, the data used to develop this study is freely available on the internet and adequately referenced. During this research, there were no personal data or interviews involved at any point in the process.

Two meetings with the SGC and Pontificia Universidad Javeriana took place between September and October 2020. Several aspects regarding their project for the torrential flow hazard at medium and detailed scale were discussed. However, they provided no data, and the discussed details are not treated in this document.

LIST OF REFERENCES

- Arango, M. I., Aristizábal, E., & Gómez, F. (2020). Morphometrical analysis of torrential flows-prone catchments in tropical and mountainous terrain of the Colombian Andes by machine learning techniques. *Natural Hazards*, 1–30. <https://doi.org/10.1007/s11069-020-04346-5>
- Aristizábal, E., Arango, M. I., Gómez, F. J., López Castro, S. M., De Villeros Severiche, A., & Riaño Quintanilla, A. F. (2020). Hazard analysis of hydrometeorological concatenated processes in the Colombian Andes. In F. Fernandes, A. Malheiro, & H. Chaminé (Eds.), *Advances in Natural Hazards and Hydrological Risks: Meeting the Challenge*. (pp. 7–10). https://doi.org/10.1007/978-3-030-34397-2_2
- Aristizábal, E., Arango, M. I., & López, I. K. G. (2020). Definition and classification of torrential avenues and their impact in the Colombian Andes. *Cuadernos de Geografía: Revista Colombiana de Geografía*, 29(1), 242–258. <https://doi.org/10.15446/rcdg.v29n1.72612>
- Aristizábal, E., & Sánchez, O. (2020). Spatial and temporal patterns and the socioeconomic impacts of landslides in the tropical and mountainous Colombian Andes. *Disasters*, 44(3), 596–618. <https://doi.org/10.1111/disa.12391>
- Bahrami, Y., Hassani, H., & Maghsoudi, A. (2020). Landslide susceptibility mapping using AHP and fuzzy methods in the Gilan province, Iran. *GeoJournal* 2020 86:4, 86(4), 1797–1816. <https://doi.org/10.1007/S10708-020-10162-Y>
- Bakka, H., Rue, H., Fuglstad, G.-A., Riebler, A., Bolin, D., Illian, J., ... Lindgren, F. (2018). Spatial modeling with R-INLA: A review. *Wiley Interdisciplinary Reviews: Computational Statistics*, 10(6), e1443. <https://doi.org/10.1002/WICS.1443>
- Ballabio, C., & Sterlacchini, S. (2012). Support vector machines for landslide susceptibility mapping: The Staffora river basin case study, Italy. *Mathematical Geosciences* 2011 44:1, 44(1), 47–70. <https://doi.org/10.1007/S11004-011-9379-9>
- Barbosa, N., Andreani, L., Gloaguen, R., & Ratschbacher, L. (2021). Window-based morphometric indices as predictive variables for landslide susceptibility models. *Remote Sensing* 2021, Vol. 13, Page 451, 13(3), 451. <https://doi.org/10.3390/RS13030451>
- Borga, M., Stoffel, M., Marchi, L., Marra, F., & Jakob, M. (2014). Hydrogeomorphic response to extreme rainfall in headwater systems: Flash floods and debris flows. *Journal of Hydrology*, 518(PB), 194–205. <https://doi.org/10.1016/J.JHYDROL.2014.05.022>
- Bout, B., Lombardo, L., van Westen, C. J., & Jetten, V. G. (2018). Integration of two-phase solid fluid equations in a catchment model for flashfloods, debris flows and shallow slope failures. *Environmental Modelling and Software*. <https://doi.org/10.1016/j.envsoft.2018.03.017>
- Brenning, A. (2005). Spatial prediction models for landslide hazards: review, comparison and evaluation. *Natural Hazards and Earth System Sciences*, 5, 853–862.
- Cardona, A., Valencia, V., Bustamante, C., García-Casco, A., Ojeda, G., Ruiz, J., ... Weber, M. (2010). Tectonomagmatic setting and provenance of the Santa Marta Schists, northern Colombia: Insights on the growth and approach of Cretaceous Caribbean oceanic terranes to the South American continent. *Journal of South American Earth Sciences*, 29(4), 784–804. <https://doi.org/10.1016/J.JSAMES.2009.08.012>
- Carey, M. (2008). Disasters, development, and glacial lake control in twentieth-century Peru. In *Advances in Global Change Research* (Vol. 31, pp. 181–196). https://doi.org/10.1007/978-1-4020-6748-8_11
- Carvajal Perico, J. H. (2012). Propuesta de estandarización de la cartografía geomorfológica en Colombia. In Servicio Geológico Colombiano (Ed.), *Propuesta de estandarización de la cartografía geomorfológica en Colombia*. <https://doi.org/10.32685/9789589952825>
- Castellanos Abella, E. A., & Van Westen, C. J. (2007). Generation of a landslide risk index map for Cuba using spatial multi-criteria evaluation. *Landslides* 2007 4:4, 4(4), 311–325. <https://doi.org/10.1007/S10346-007-0087-Y>
- Castillo, L. A., & Vargas, G. (2013). Seismostratigraphy of Los Cayos basin. *Boletín de Geología*, 35, 8.
- Chen, W., Pourghasemi, H. R., Panahi, M., Kornejady, A., Wang, J., Xie, X., & Cao, S. (2017). Spatial prediction of landslide susceptibility using an adaptive neuro-fuzzy inference system combined with frequency ratio, generalized additive model, and support vector machine techniques. *Geomorphology*, 297, 69–85. <https://doi.org/10.1016/J.GEOMORPH.2017.09.007>
- Choudhari, P. P., Nigam, G. K., Singh, S. K., & Thakur, S. (2018). Morphometric based prioritization of watershed for groundwater potential of Mula river basin, Maharashtra, India. *Geology, Ecology, and Landscapes*, 2(4). <https://doi.org/10.1080/24749508.2018.1452482>

- Constantin, M., Bednarik, M., Jurchescu, M. C., & Vlaicu, M. (2010). Landslide susceptibility assessment using the bivariate statistical analysis and the index of entropy in the Sibiciu Basin (Romania). *Environmental Earth Sciences* 2010 63:2, 63(2), 397–406. <https://doi.org/10.1007/S12665-010-0724-Y>
- Cruden, D. M., & Varnes, D. J. (1996). Landslide types and processes. In *Landslides, investigation and mitigation*. Washington D.C.: Transportation Research Board.
- Dowling, C. A., & Santi, P. M. (2013). Debris flows and their toll on human life: a global analysis of debris-flow fatalities from 1950 to 2011. *Natural Hazards* 2013 71:1, 71(1), 203–227. <https://doi.org/10.1007/S11069-013-0907-4>
- Ermini, L., Catani, F., & Casagli, N. (2005). Artificial neural networks applied to landslide susceptibility assessment. *Geomorphology*, 66(1–4), 327–343. <https://doi.org/10.1016/J.GEOMORPH.2004.09.025>
- Farr, T. G., Rosen, P. A., Caro, E., Crippen, R., Duren, R., Hensley, S., ... Alsdorf, D. E. (2007). The shuttle radar topography mission. *Reviews of Geophysics*, 45(2). <https://doi.org/10.1029/2005RG000183>
- Froude, M. J., & Petley, D. N. (2018). Global fatal landslide occurrence from 2004 to 2016. *Natural Hazards and Earth System Sciences*, 18(8), 2161–2181. <https://doi.org/10.5194/nhess-18-2161-2018>
- Funk, C., Peterson, P., Landsfeld, M., Pedreros, D., Verdin, J., Shukla, S., ... Michaelsen, J. (2015). The climate hazards infrared precipitation with stations - A new environmental record for monitoring extremes. *Scientific Data*, 2(1), 1–21. <https://doi.org/10.1038/sdata.2015.66>
- Galli, M., Ardizzone, F., Cardinali, M., Guzzetti, F., & Reichenbach, P. (2008). Comparing landslide inventory maps. *Geomorphology*, 94(3–4), 268–289. <https://doi.org/10.1016/j.geomorph.2006.09.023>
- Goetz, J. N., Brenning, A., Petschko, H., & Leopold, P. (2015). Evaluating machine learning and statistical prediction techniques for landslide susceptibility modeling. *Computers & Geosciences*, 81, 1–11. <https://doi.org/10.1016/J.CAGEO.2015.04.007>
- Gómez Tapias, J., Núñez-tello, A., Mateus-zabala, D., Alirio ALCÁRCEL-GUTIÉRREZ, F., Melissa LASSO-MUÑOZ, R., Marín-rincón, E., & Paula MARROQUÍN-GÓMEZ, M. (2020). *Physiographic and geological setting of the Colombian territory*. 16. <https://doi.org/10.32685/pub.esp.35.2019.01>
- Güneralp, B., Güneralp, I., & Liu, Y. (2015). Changing global patterns of urban exposure to flood and drought hazards. *Global Environmental Change*, 31, 217–225. <https://doi.org/10.1016/j.gloenvcha.2015.01.002>
- Guzzetti, F. (2006). *Landslide hazard and risk assessment*. University of Bonn, Bonn, Germany.
- Guzzetti, F., Mondini, A. C., Cardinali, M., Fiorucci, F., Santangelo, M., & Chang, K. T. (2012, April). Landslide inventory maps: New tools for an old problem. *Earth-Science Reviews*, Vol. 112, pp. 42–66. <https://doi.org/10.1016/j.earscirev.2012.02.001>
- Guzzetti, F., Reichenbach, P., Ardizzone, F., Cardinali, M., & Galli, M. (2006). Estimating the quality of landslide susceptibility models. *Geomorphology*, 81(1–2), 166–184. <https://doi.org/10.1016/J.GEOMORPH.2006.04.007>
- Guzzetti, F., Reichenbach, P., Cardinali, M., Galli, M., & Ardizzone, F. (2005). Probabilistic landslide hazard assessment at the basin scale. *Geomorphology*, 72(1–4), 272–299. <https://doi.org/10.1016/j.geomorph.2005.06.002>
- Hervás, J., & Bobrowsky, P. (2009). Mapping: inventories, susceptibility, hazard and risk. In K. Sassa & P. Canuti (Eds.), *Landslides -- Disaster Risk Reduction* (pp. 321–349). https://doi.org/10.1007/978-3-540-69970-5_19
- Horton, R. E. (1932). Drainage-basin characteristics. *Eos, Transactions American Geophysical Union*, 13(1), 350–361. <https://doi.org/10.1029/TR013i001p00350>
- Horton, R. E. (1945). Erosional development of streams and their drainage basins; Hydrophysical approach to quantitative morphology. *Bulletin of the Geological Society of America*, 56(3), 275–370. [https://doi.org/10.1130/0016-7606\(1945\)56\[275:EDOSAT\]2.0.CO;2](https://doi.org/10.1130/0016-7606(1945)56[275:EDOSAT]2.0.CO;2)
- Hosmer, D. W., Lemeshow, S., & Sturdivant, R. X. (2013). Applied Logistic Regression: Third Edition. *Applied Logistic Regression: Third Edition*, 1–510. <https://doi.org/10.1002/9781118548387>
- Hungr, O., Evans, S. G., Bovis, M. J., & Hutchinson, J. N. (2001). A review of the classification of landslides of the flow type. *Environmental and Engineering Geoscience*, 7(3), 221–238. <https://doi.org/10.2113/GSEEGEOSCI.7.3.221>
- Hungr, O., & Jakob, M. (2005). Debris-flow hazards and related phenomena. In *Debris-flow Hazards and Related Phenomena*. <https://doi.org/10.1007/b138657>
- Hungr, O., Leroueil, S., & Picarelli, L. (2014, November 30). The Varnes classification of landslide types, an update. *Landslides*, Vol. 11, pp. 167–194. <https://doi.org/10.1007/s10346-013-0436-y>
- IDEAM. (2010). *Leyenda nacional de coberturas de la tierra. Metodología CORINE Land Cover adaptada para*

- Colombia, escala 1:100.000* (N. J. Martínez Ardila & U. G. Murcia García, Eds.). Bogotá.
- IDEAM. (2013). *Zonificación y codificación de unidades hidrográficas e hidrogeológicas de Colombia* (N. O. Vargas Martínez & M. García Herrán, Eds.). Bogotá.
- IDEAM. (2017). Guía metodológica para la elaboración de mapas de inundación. In *Guía metodológica para la elaboración de mapas de inundación, Colombia*. Retrieved from http://documentacion.ideam.gov.co/openbiblio/bvirtual/023774/GUIA_METODOLOGICA_MAPAS_INUNDACION_MARZO_2018.pdf
- Ilanloo, M. (2011). A comparative study of fuzzy logic approach for landslide susceptibility mapping using GIS: An experience of Karaj dam basin in Iran. *Procedia - Social and Behavioral Sciences*, 19, 668–676. <https://doi.org/10.1016/J.SBSPRO.2011.05.184>
- Islam, A., & Deb Barman, S. (2020). Drainage basin morphometry and evaluating its role on flood-inducing capacity of tributary basins of Mayurakshi River, India. *SN Applied Sciences* 2020 2:6, 2(6), 1–23. <https://doi.org/10.1007/S42452-020-2839-4>
- Iverson, R. M. (2005). Debris-flow mechanics. *Debris-Flow Hazards and Related Phenomena*, 105–134. https://doi.org/10.1007/3-540-27129-5_6
- Jakob, M., & Hungr, O. (2005). Debris-flow hazards and related phenomena. In *Debris-flow Hazards and Related Phenomena*. <https://doi.org/10.1007/b138657>
- Kayastha, P., Dhital, M. R., & De Smedt, F. (2013). Application of the analytical hierarchy process (AHP) for landslide susceptibility mapping: A case study from the Tinau watershed, west Nepal. *Computers and Geosciences*, 52, 398–408. <https://doi.org/10.1016/j.cageo.2012.11.003>
- Khan, M. I., & Wang, S. (2021). Slope stability analysis to correlate shear strength with slope angle and shear stress by considering saturated and unsaturated seismic conditions. *Applied Sciences* 2021, Vol. 11, Page 4568, 11(10), 4568. <https://doi.org/10.3390/APP11104568>
- Komendantova, N., Mrzyglocki, R., Mignan, A., Khazai, B., Wenzel, F., Patt, A., & Fleming, K. (2014). Multi-hazard and multi-risk decision-support tools as a part of participatory risk governance: Feedback from civil protection stakeholders. *International Journal of Disaster Risk Reduction*, 8, 50–67. <https://doi.org/10.1016/j.ijdr.2013.12.006>
- Larsen, M. C., Wiczorek, G. F., Eaton, L. S., Morgan, B. A., & Torres-Sierra, H. (2001). Venezuelan debris flow and flash flood disaster of 1999 studied. *Eos, Transactions American Geophysical Union*, 82(47), 572–572. <https://doi.org/10.1029/01EO00335>
- Lin, M. L., & Tung, C. C. (2004). A GIS-based potential analysis of the landslides induced by the Chi-Chi earthquake. *Engineering Geology*, 71(1–2), 63–77. [https://doi.org/10.1016/S0013-7952\(03\)00126-1](https://doi.org/10.1016/S0013-7952(03)00126-1)
- Lombardo, L., Opitz, T., Ardizzone, F., Guzzetti, F., & Huser, R. (2020, October 1). Space-time landslide predictive modelling. *Earth-Science Reviews*, Vol. 209, p. 103318. <https://doi.org/10.1016/j.earscirev.2020.103318>
- Lombardo, L., Opitz, T., & Huser, R. (2018). Point process-based modeling of multiple debris flow landslides using INLA: an application to the 2009 Messina disaster. *Stochastic Environmental Research and Risk Assessment*, 32(7), 2179–2198. <https://doi.org/10.1007/s00477-018-1518-0>
- Lombardo, L., Tanyas, H., & Nicu, I. C. (2020). Spatial modeling of multi-hazard threat to cultural heritage sites. *Engineering Geology*, 277, 105776. <https://doi.org/10.1016/j.enggeo.2020.105776>
- Mark, D. M. (1975). Geomorphometric Parameters: A Review and Evaluation. *Geografiska Annaler. Series A, Physical Geography*, 57(3/4), 165. <https://doi.org/10.2307/520612>
- Martino, S., & Riebler, A. (2019). Integrated Nested Laplace Approximations (INLA). *ArXiv: Computation*, 19. <https://doi.org/10.1002/9781118445112.stat08212>
- Matauco, A. I. G. De. (2004). Análisis morfométrico de la cuenca y de la red de drenaje del río Zadorra y sus afluentes aplicado a la peligrosidad de crecidas. *Boletín de La Asociación de Geógrafos Españoles*, 0(38). Retrieved from <https://bage.age-geografia.es/ojs/index.php/bage/article/view/495>
- Meena, S. R., Mishra, B. K., & Piralilou, S. T. (2019). A hybrid spatial multi-criteria evaluation method for mapping landslide susceptible areas in Kullu valley, Himalayas. *Geosciences* 2019, Vol. 9, Page 156, 9(4), 156. <https://doi.org/10.3390/GEOSCIENCES9040156>
- Murillo-García, F. G., & Alcántara-Ayala, I. (2015). Landslide susceptibility analysis and mapping using statistical multivariate techniques: Pahuatlán, Puebla, Mexico. In W. Wu (Ed.), *Recent Advances in Modeling Landslides and Debris Flows* (pp. 179–194). https://doi.org/10.1007/978-3-319-11053-0_16
- Nadim, F., Kjekstad, O., Peduzzi, P., Herold, C., & Jaedicke, C. (2006, May 8). Global landslide and avalanche hotspots. *Landslides*, Vol. 3, pp. 159–173. <https://doi.org/10.1007/s10346-006-0036-1>
- Nelder, J. A., & Wedderburn, R. W. M. (1972). Generalized linear models. *Journal of the Royal Statistical Society. Series A (General)*, 135(3), 370. <https://doi.org/10.2307/2344614>

- Palazzolo, N., Peres, D. J., Bordoni, M., Meisina, C., Creaco, E., & Cancelliere, A. (2021). Improving spatial landslide prediction with 3D slope stability analysis and genetic algorithm optimization: application to the Oltrepò Pavese. *Water* 2021, Vol. 13, Page 801, 13(6), 801. <https://doi.org/10.3390/W13060801>
- Petschko, H., Brenning, A., Bell, R., Goetz, J., & Glade, T. (2014). Assessing the quality of landslide susceptibility maps-case study Lower Austria. *Hazards Earth Syst. Sci*, 14, 95–118. <https://doi.org/10.5194/nhess-14-95-2014>
- Poveda, G., Vélez, J. I., Mesa, O. J., Cuartas, A., Barco, J., Mantilla, R. I., ... Quevedo, D. I. (2007). Linking long-term water balances and statistical scaling to estimate river flows along the drainage network of Colombia. *Journal of Hydrologic Engineering*, 12(1), 4–13. [https://doi.org/10.1061/\(ASCE\)1084-0699\(2007\)12:1\(4\)](https://doi.org/10.1061/(ASCE)1084-0699(2007)12:1(4))
- Pulido, N. (2003). Seismotectonics of the northern Andes (Colombia) and the development of seismic networks. *Bulletin of the International Institute of Seismology and Earthquake Engineering*, 69–76.
- Reichenbach, P., Rossi, M., Malamud, B. D., Mihir, M., & Guzzetti, F. (2018, May 1). A review of statistically-based landslide susceptibility models. *Earth-Science Reviews*, Vol. 180, pp. 60–91. <https://doi.org/10.1016/j.earscirev.2018.03.001>
- Rogelis, M. C., & Werner, M. (2014). Regional debris flow susceptibility analysis in mountainous peri-urban areas through morphometric and land cover indicators. *Natural Hazards and Earth System Sciences*, 14(11), 3043–3064. <https://doi.org/10.5194/nhess-14-3043-2014>
- Rossi, M., & Reichenbach, P. (2016). LAND-SE: a software for statistically based landslide susceptibility zonation, version 1.0. *Geoscientific Model Development*, 9(10), 3533–3543. <https://doi.org/10.5194/gmd-9-3533-2016>
- Rue, H., Martino, S., & Chopin, N. (2009). Approximate Bayesian inference for latent Gaussian models by using integrated nested Laplace approximations. *Journal of the Royal Statistical Society. Series B: Statistical Methodology*, 71(2), 319–392. <https://doi.org/10.1111/j.1467-9868.2008.00700.x>
- Ruff, M., & Czurda, K. (2008). Landslide susceptibility analysis with a heuristic approach in the Eastern Alps (Vorarlberg, Austria). *Geomorphology*, 94(3–4), 314–324. <https://doi.org/10.1016/j.geomorph.2006.10.032>
- Saadatkah, N., Mansor, S., Kassim, A., Lee, L. M., Saadatkah, R., & Sobhanmanesh, A. (2016). Regional modeling of rainfall-induced landslides using TRIGRS model by incorporating plant cover effects: case study in Hulu Kelang, Malaysia. *Environmental Earth Sciences* 2016 75:5, 75(5), 1–20. <https://doi.org/10.1007/S12665-016-5326-X>
- Schumm, S. A. (1956). Evolution of drainage systems and slopes in badlands at Perth Amboy, New Jersey. *Bulletin of the Geological Society of America*, 67(5), 597–646. [https://doi.org/10.1130/0016-7606\(1956\)67\[597:EODSAS\]2.0.CO;2](https://doi.org/10.1130/0016-7606(1956)67[597:EODSAS]2.0.CO;2)
- Sepúlveda, S. A., Rebolledo, S., & Vargas, G. (2006). Recent catastrophic debris flows in Chile: geological hazard, climatic relationships and human response. *Quaternary International*, 158(1), 83–95. <https://doi.org/10.1016/j.quaint.2006.05.031>
- Servicio Geológico Colombiano. (2012). *Guía metodológica para la zonificación de susceptibilidad y amenaza relativa por movimientos en masa, escala 1 : 100.000*. <https://doi.org/10.13140/RG.2.2.18425.47203>
- Servicio Geológico Colombiano. (2015). *Guía metodológica para estudios de amenaza, vulnerabilidad y riesgo por movimientos en masa*. Bogotá.
- Servicio Geológico Colombiano, & Pontificia Universidad Javeriana. (2020). *Documento preliminar guía metodológica para zonificación de amenaza por avenidas torrenciales*. Bogotá.
- Sevgen, Kocaman, Nefeslioglu, & Gokceoglu. (2019). A Novel Performance Assessment Approach using Photogrammetric Techniques for landslide susceptibility mapping with logistic regression, ANN and random forest. *Sensors*, 19(18), 3940. <https://doi.org/10.3390/s19183940>
- Steger, S., Brenning, A., Bell, R., & Glade, T. (2017). The influence of systematically incomplete shallow landslide inventories on statistical susceptibility models and suggestions for improvements. *Landslides*, 14(5), 1767–1781. <https://doi.org/10.1007/s10346-017-0820-0>
- Steger, Stefan, Brenning, A., Bell, R., & Glade, T. (2016). The propagation of inventory-based positional errors into statistical landslide susceptibility models. *Hazards Earth Syst. Sci*, 16, 2729–2745. <https://doi.org/10.5194/nhess-16-2729-2016>
- Steger, Stefan, Brenning, A., Bell, R., Petschko, H., & Glade, T. (2016). Exploring discrepancies between quantitative validation results and the geomorphic plausibility of statistical landslide susceptibility maps. *Geomorphology*, 262, 8–23. <https://doi.org/10.1016/j.geomorph.2016.03.015>
- Van Westen, C. J., Rengers, N., & Soeters, R. (2003). Use of geomorphological information in indirect

- landslide susceptibility assessment. *Natural Hazards*, 30(3), 399–419. <https://doi.org/10.1023/B:NHAZ.0000007097.42735.9e>
- Villacorta, S. P., Evans, K. G., Nakatani, K., & Villanueva, I. (2020). Large debris flows in Chosica, Lima, Peru: the application of hydraulic infrastructure for erosion control and disaster prevention. *Australian Journal of Earth Sciences*, 67(3), 425–436. <https://doi.org/10.1080/08120099.2020.1690577>
- Voight, B. (1990). The 1985 Nevado del Ruiz volcano catastrophe: anatomy and retrospection. *Journal of Volcanology and Geothermal Research*, 42(1–2), 151–188. [https://doi.org/10.1016/0377-0273\(90\)90075-Q](https://doi.org/10.1016/0377-0273(90)90075-Q)
- Wang, N., Cheng, W., Lombardo, L., Xiong, J., & Guo, L. (2021). Statistical spatiotemporal analysis of hydro-morphological processes in China during 1950–2015. *Stochastic Environmental Research and Risk Assessment*. <https://doi.org/10.1007/s00477-021-02007-y>
- Welsh, A. (2007). *Delineating debris-flow hazards on alluvial fans in the Coromandel and Kaimai regions, New Zealand using GIS Non-technical Summary*. University of Canterbury, Canterbury.
- Wilford, D. J., Sakals, M. E., Innes, J. L., Sidle, R. C., & Bergerud, W. A. (2004). Recognition of debris flow, debris flood and flood hazard through watershed morphometrics. *Landslides*, 1(1), 61–66. <https://doi.org/10.1007/s10346-003-0002-0>
- Wohl, E. E., & Pearthree, P. P. (1991). Debris flows as geomorphic agents in the Huachuca Mountains of southeastern Arizona. *Geomorphology*, 4(3–4), 273–292. [https://doi.org/10.1016/0169-555X\(91\)90010-8](https://doi.org/10.1016/0169-555X(91)90010-8)
- Zhang, S., Zhang, L. M., & Glade, T. (2014). Characteristics of earthquake- and rain-induced landslides near the epicenter of Wenchuan earthquake. *Engineering Geology*, 175, 58–73. <https://doi.org/10.1016/j.enggeo.2014.03.012>

10. APPENDIX

10.1. Land cover parametrization

Original data		New data	
Level	Legend	New level	Name
111	Continuous urban fabric	1	Artificial land
112	Discontinuos urban fabric	1	Artificial land
121	Industrial and commercial units	1	Artificial land
122	Road and rail networks	122	Roads and railroads
123	Ports	1	Artificial surfaces
124	Airports	1	Artificial surfaces
125	Obras hidraulicas	1	Artificial surfaces
131	Mineral extraction zones	13	Mine, dump and construction sites
132	Dump sites	13	Mine, dump and construction sites
141	Green urban areas	1	Artificial surfaces
142	Sport and leisure facilities	1	Artificial surfaces
211	Non-irrigated arable land	21	Arable land
212	Cereals	21	Arable land
213	Oliseeds and legumes	21	Arable land
214	Vegetables	21	Arable land
215	Tubers	21	Arable land
221	Herbaceous permanent crops	22	Permanent crops
222	Bushy permanent crops	22	Permanent crops
223	Arboreal permanent crops	22	Permanent crops
224	Agroforestry crops	22	Permanent crops
225	Confined crops	22	Permanent crops
231	Pastures	23	Grassland
232	Arboreal pastures	23	Grassland
233	Bushy pastures	23	Grassland
241	Annual crops associated with permanent crops	24	Heterogeneous agricultural areas
242	Annual crops associated with permanent pastures	24	Heterogeneous agricultural areas
243	Crops, pastures and natural spaces	24	Heterogeneous agricultural areas
244	Pastures and natural spaces	24	Heterogeneous agricultural areas
245	Crops with natural spaces	24	Heterogeneous agricultural areas
311	Dense forest	311	Dense forest
312	Open forest	312	Open forest
313	Fragmented forest	313	Fragmented forest
314	Riparian forest	314	Riparian forest
315	Forest plantation	315	Forest plantation
321	Herbaceous vegetation	32	Shrub/herbaceous vegetation associations
322	Bushes	32	Shrub/herbaceous vegetation associations
323	Transitional woodland-shrubs	32	Shrub/herbaceous vegetation associations
331	Beaches, dune, sands	331	Beaches, dunes, sands
332	Bare rocks	332	Bare rock
333	Badlands	333	Badlands

334	Burnt areas	334	Burned areas
335	Glaciers and perpetual snow	335	Glaciers and perpetual snow
411	Inland marshes	41	Inland wetlands
412	Peat bogs	41	Inland wetlands
413	Aquatic vegetation	41	Inland wetlands
421	Salt marshes	42	Coastal wetlands
422	Salines	42	Coastal wetlands
423	Intertidal flats	42	Coastal wetlands
511	Water courses	51	Inland waters
512	Water bodies	51	Inland waters
513	Waterways	51	Inland waters
514	Artificial water bodies	51	Inland waters
521	Coastal lagoons	52	Marine waters
522	Sea and oceans	52	Marine waters
523	Estuaries	52	Marine waters
999	Clouds	9	Clouds

10.2. Potential land use

Potential use	New class
Permanent intensive crops in warm weather	Agriculture
Permanent intensive crops in cold weather	Agriculture
Permanent intensive crops in semi-warm weather	Agriculture
Permanent semi-intensive crops in warm weather	Agriculture
Permanent semi-intensive crops in cold weather	Agriculture
Permanent semi-intensive crops in semi-warm weather	Agriculture
Transitory intensive crops in warm weather	Agriculture
Transitory intensive crops in cold weather	Agriculture
Transitory intensive crops in warm weather	Agriculture
Transitory semi-intensive crops in warm weather	Agriculture
Transitory semi-intensive crops in cold weather	Agriculture
Transitory semi-intensive crops in semi-warm weather	Agriculture
Agrosilvícola con cultivos permanentes	Agroforestry
Agrosilvícola con cultivos transitorios	Agroforestry
Agrosilvopastoril con cultivos permanentes	Agroforestry
Agrosilvopastoril con cultivos transitorios	Agroforestry
Extensive pasture in warm weather	Animal husbandry
Extensive pasture in cold weather	Animal husbandry
Extensive pasture in semi-warm weather	Animal husbandry
Intensive pasture in warm weather	Animal husbandry
Intensive pasture in cold weather	Animal husbandry
Intensive pasture in semi-warm weather	Animal husbandry
Semi-intensive pasture in warm weather	Animal husbandry
Semi-intensive pasture in cold weather	Animal husbandry
Semi-intensive pasture in semi-warm weather	Animal husbandry
Dunes	Conservation
Hydrological resources conservation	Conservation
Hydrobiological resources conservation	Conservation
Conservation and erosion recovery	Conservation

Conservation and salinity recovery	Conservation
Salines	Conservation
Forest production warm weather	Forest production
Forest production cold weather	Forest production
Forest production semi-warm weather	Forest production
Forest production very cold weather	Forest production
Forestral protection	Forest protection
Protection - production	Forest protection
Dump	Infrastructure
Quarry	Infrastructure
Coal mine	Infrastructure
Dam	Infrastructure
Coal tailings	Infrastructure
Airport	Residential areas
Military base	Residential areas
Building	Residential areas
Urban fabric	Residential areas
Silvopasture	Silvopasture
Water body	Water body

10.3. Daily rainfall data preparation

```
// Import boundary
var Colombia = table2.filter(ee.Filter.inList("COUNTRY_NAME", ["Colombia"]))
Map.addLayer(Colombia)
var lng = -75.57370054106894;
var lat = 6.256322268469186;
var point = ee.Geometry.Point([lng, lat]);

// Import, filter and apply reducer function
var rainfall_mean = ee.ImageCollection("UCSB-CHG/CHIRPS/DAILY")
.select('precipitation')
.filterDate('1981-01-01', '2020-12-31')
.mean();

var rainfall_max = ee.ImageCollection("UCSB-CHG/CHIRPS/DAILY")
.select('precipitation')
.filterDate('1981-01-01', '2020-12-31')
.max();

var rainfall_sum = ee.ImageCollection("UCSB-CHG/CHIRPS/DAILY")
.select('precipitation')
.filterDate('2011-01-01', '2011-12-31')
.sum();

// Display rainfall data
var rainfall_palette = 'ff0000, ffffff, 0000ff';
//Map.addLayer(rainfall_mean.clip(Colombia), {'min':2, 'max':22, 'palette':rainfall_palette}, 'Rainfall
mean');
```

```
Map.addLayer(rainfall_sum.clip(Colombia), {'min':321, 'max':9253, 'palette':rainfall_palette}, 'Rainfall
sum')
//Map.addLayer(rainfall_max.clip(Colombia), {'min':2, 'max':22, 'palette':rainfall_palette}, 'Rainfall max');

// Define scale to export rainfall data
var NomScale = rainfall_mean.projection().nominalScale()
print('Scale in meters:', NomScale);
//print(ui.Chart.image.series(rainfall_mean, point), ee.Reducer.mean());
//print(ui.Chart.image.series(rainfall_mean, Colombia), ee.Reducer.mean());
//print(ui.Chart.image.series(rainfall_mean, Colombia, ee.Reducer.mean(), 1));

// Export the TIFF file, specifying resolution
Export.image.toDrive({
  image: rainfall_mean,
  region: Colombia,
  description: 'CHIRPS_mean_Colombia_1981_2020_5km',
  scale: (NomScale.getInfo()*0.05),
  maxPixels: 10000000000000,
  folder : 'CHIRPS'
});
```

10.4. Annual rainfall data preparation

```
// Get boundary
var Colombia = table2.filter(ee.Filter.inList("country_na", ["Colombia"]))
Map.addLayer(Colombia)
Map.centerObject(Colombia, 5)

// Import CHIRPS and boundary
var CHIRPS = ee.ImageCollection("UCSB-CHG/CHIRPS/DAILY");

// Set start and end year
var start_year = 1981;
var end_year = 2020;

// Make a date object
var start_date = ee.Date.fromYMD(start_year, 1, 1);
var end_date = ee.Date.fromYMD(end_year + 1, 1, 1);

// Make a list with years
var years = ee.List.sequence(start_year, end_year);

// Calculate yearly precipitation
var annualPrecip = ee.ImageCollection.fromImages(years.map(function (year) {
  var annual = CHIRPS.filter(ee.Filter.calendarRange(year, year, 'year')).sum();
  return annual
  .set('year', year)
  .set('system:time_start', ee.Date.fromYMD(year, 1, 1));
}));
```

```
});  
var title = {title: 'Annual precipitation', hAxis: {title: 'Time'}, vAxis: {title: 'Precipitation (mm)'},};  
  
// Print the chart with the annual precipitation  
var chart = ui.Chart.image.seriesByRegion({  
  imageCollection: annualPrecip,  
  regions: Colombia,  
  reducer: ee.Reducer.sum(),  
  band: 'precipitation',  
  scale: 5000,  
  xProperty: 'system:time_start',  
  seriesProperty: 'SITE'  
}).setOptions(title)  
  .setChartType('ColumnChart');  
print(chart);  
  
// Calculate mean  
var annualMean = annualPrecip.mean().clip(Colombia);  
var annualMax = annualPrecip.max().clip(Colombia);  
  
// Show map  
var pViz = {min: 2000, max: 5500, palette: '000000, 0000FF, FDFF92, FF2700, FF00E7'};  
  
//Map.centerObject(Colombia, 5);  
Map.addLayer(annualMean, pViz, 'mean yearly P');  
Map.addLayer(annualMax, pViz, 'max yearly P');  
var NomScale = annualMean.projection().nominalScale();  
print('Scale in meters:', NomScale);  
  
//Export the image, specifying scale and region.  
Export.image.toDrive({  
  image: annualMean,  
  region: Colombia2,  
  description: 'annualMean_Colombia_CHIRPS',  
  scale: (NomScale.getInfo()*0.05),  
  maxPixels: 1000000000000000,  
  folder : 'CHIRPS'  
});  
  
//Export the image, specifying scale and region.  
Export.image.toDrive({  
  image: annualMax,  
  region: Colombia,  
  description: 'annualMax_Colombia_CHIRPS',  
  scale: (NomScale.getInfo()*0.05),  
  maxPixels: 1000000000000000,  
  folder : 'CHIRPS'  
});
```

10.5. Watershed generation

Initialize with archives elevation, provincias, stream_100_raster, streamv_100_vector

#set region

g.region -p raster=elevation@PERMANENT

#define watershed threshold/ define memory to be used

r.watershed -s -4 -a --overwrite elevation=elevation@PERMANENT threshold=50000
accumulation=accumulation basin=basins_50000 memory=1000

#convert basins to vector

r.to.vect input=basins_50000@PERMANENT output=basins_50000 type=area

#select basins inside provincias

v.select ainput=basins_50000@PERMANENT binput=provincias@PERMANENT
output=basinspoly_50000 operator=intersects

#set mask

r.mask vector=basinspoly_50000@PERMANENT

#clip drainages to the selected basins

v.clip input=streamv_100r@PERMANENT clip=basinspoly_50000@PERMANENT
output=streamv_100r_50000

#export points

v.out.ogr input=streamatt_100@PERMANENT type=point
output=D:\ITC\0_Thesis\Watershed\Colombia\streamatt_100.gpkg format=GPKG
v.in.ogr input=D:\ITC\0_Thesis\Watershed\Colombia\streamatt_100.gpkg
output=streamatt_100_point
v.clip input=streamatt_100_point@PERMANENT clip=basinspoly_50000@PERMANENT
output=streamatt_100_point_50000

#attributes to the new points

v.db.addcolumn map=streamatt_100_point_50000@PERMANENT columns="xcoor double precision,
ycoor double precision, accum double precision, height integer, basinID integer"
v.to.db map=streamatt_100_point_50000@PERMANENT option=coor columns=xcoor,ycoor --
overwrite

extract values per points

v.what.rast -i map=streamatt_100_point_50000@PERMANENT raster=accumulation@PERMANENT
column=accum
v.what.rast -i map=streamatt_100_point_50000@PERMANENT raster=elevation@PERMANENT
column=height
v.what.rast map=streamatt_100_point_50000@PERMANENT raster=basins_50000@PERMANENT
column=basinID

export points

v.out.ogr input=streamatt_100_point_50000@PERMANENT type=point
output=D:\ITC\0_Thesis\Watershed\Colombia\streamatt_100_point_50000.gpkg

```
# filter by max accumulation in QGIS
"accum" = maximum("accum","basinID")

#check unique values with 'group stats' and 'mmgis'-plugin to remove duplicated data

# import back
v.in.ogr input=D:\ITC\0_Thesis\Watershed\Colombia\streamatt_100_point_50000_accum.shp
output=streamatt_100_point_50000_accum_dup

#convert to raster
v.to.rast input=streamatt_100_point_50000_accum_dup@PERMANENT
output=streamatt_100_point_50000_accum_dupr use=attr attribute_column=basinID

# stream distance
r.stream.distance -o -s stream_rast=streamatt_100_point_50000_accum_dupr@PERMANENT
direction=direction@PERMANENT elevation=elevation@PERMANENT method=downstream
distance=distance difference=diffelevation

# Aggregate stream information per watershed
v.vect.stats points=streamatt_100_point_50000@PERMANENT
areas=basinspoly_50000@PERMANENT method=maximum points_column=strahler
count_column=strahler_count stats_column=strahler_order
```

10.6. Terrain derivatives calculation and aggregation procedure

```
#Slope
v.rast.stats map=basinspoly_1000@PERMANENT raster=slope@PERMANENT column_prefix=slope
method=average,stddev

#Profile curvature
v.rast.stats map=basinspoly_1000@PERMANENT raster=profile_curv@PERMANENT
column_prefix=profile_curv method=average,stddev

#Tangential curvature
v.rast.stats map=basinspoly_1000@PERMANENT raster=tangential_curv@PERMANENT
column_prefix=tangential_curv method=average,stddev

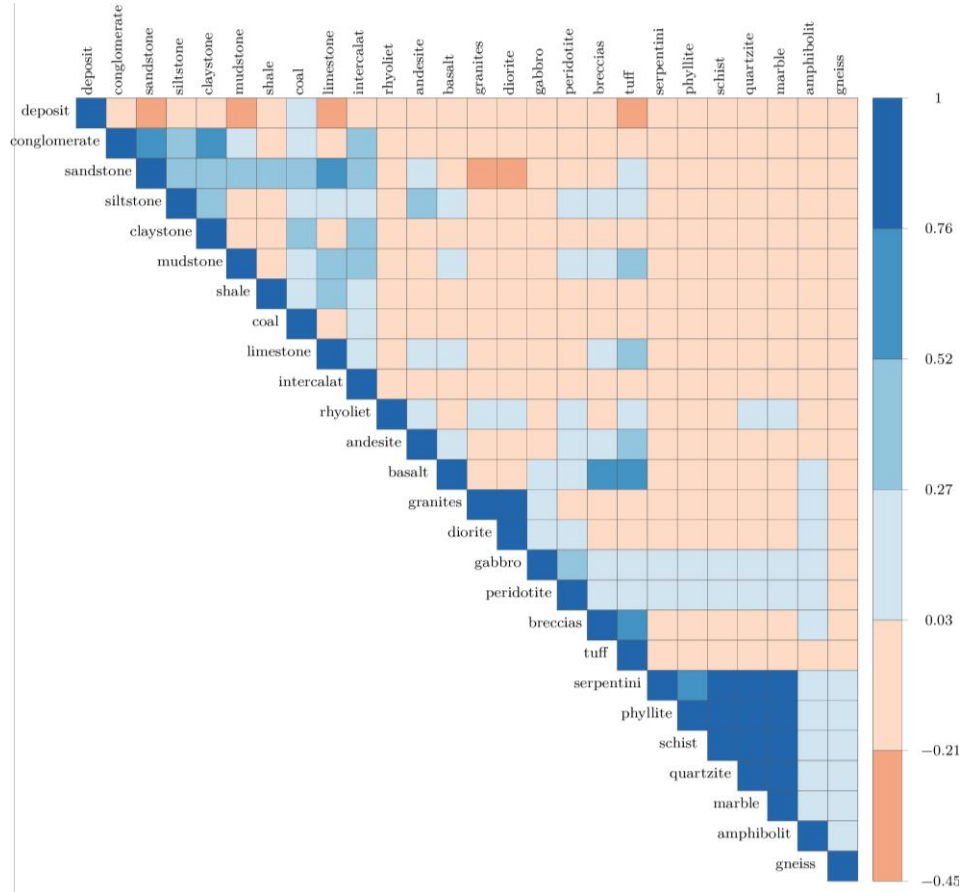
#Relief
v.rast.stats map=basinspoly_1000@PERMANENT raster=elevation@PERMANENT
column_prefix=relief method=range

#Rainfall
v.rast.stats map=basinspoly_1000@PERMANENT raster=Rainfall_daily_mean@PERMANENT
column_prefix=Rainfall_daily_mean method=average,stddev -c
v.rast.stats map=basinspoly_1000@PERMANENT raster=Rainfall_daily_max@PERMANENT
column_prefix=Rainfall_daily_max method=maximum,average,stddev -c
```

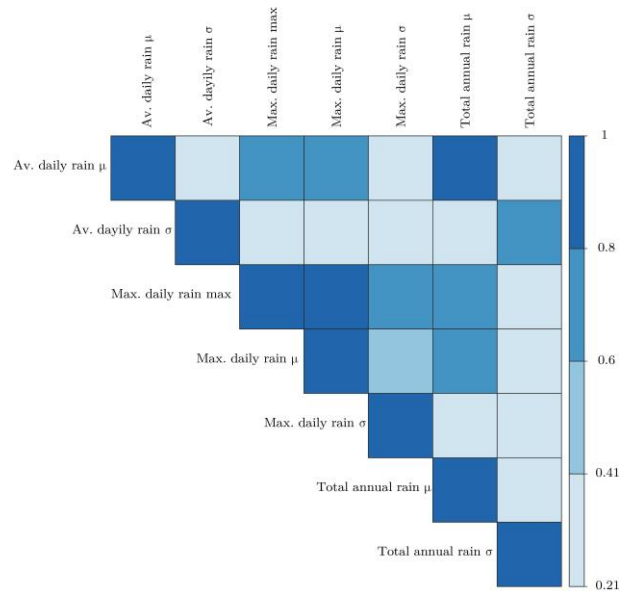
v.rast.stats map=basinspoly_1000@PERMANENT raster=Rainfall_annual_sum@PERMANENT
 column_prefix=Rainfall_annual_sum method=average,stddev

10.7. Multi-collinearity test

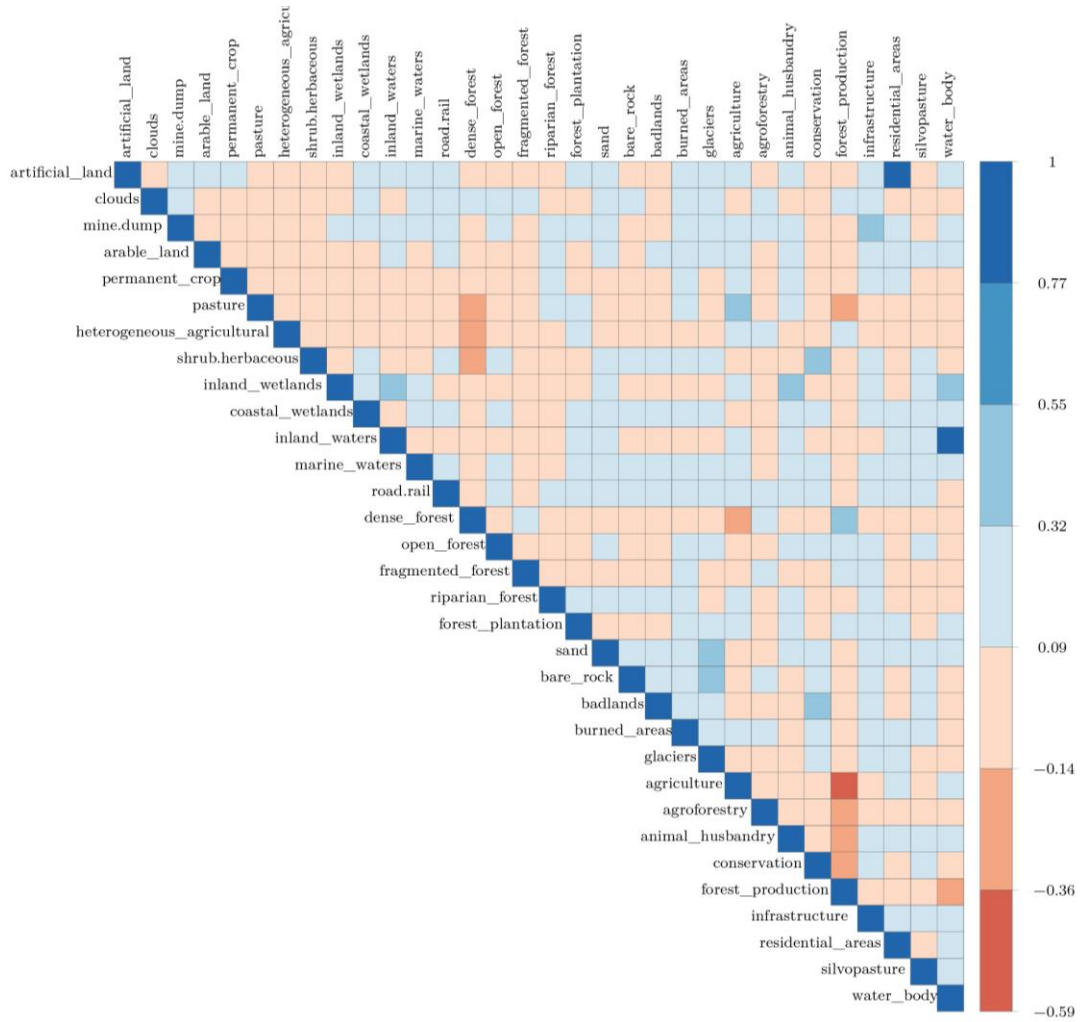
10.8. Multi-collinearity test for Geology



10.9. Multi-collinearity test for rainfall



10.10. Multi-collinearity test for land cover and land use



10.11. Posterior 95% CI vs. posterior mean susceptibilities for all the watershed levels and models

